Pressure induced tricritical point in the ferroelectric phase transition of potassium dihydrogen phosphate
by Arthur Boyd Western

A thesis submitted in partial fulfillment of the requirements for the degree of DOCTOR OF PHILOSOPHY in Physics
Montana State University

Abstract:
Measurement of the net polarization charge of a KH2PO4 crystal as a function of temperature, applied electric field, and hydrostatic pressure indicates the existence of a tricritical point near 2 kbar of pressure. This result is based upon static measurements of the polarization response to applied dc field in a 0.5 K neighborhood of the ferroelectric transition at pressures of 0, 3, and 3 kbar.

In each case the paraelectric region is well described by the Landau equation of state, E=A0(T-T0)P+BP3+CP5, to within 0.05 K of the transition temperature. Analysis of the data along lines of constant polarization, which are here called "isopols," indicate that the transition is first-order at 0 and 1 kbar with the critical field decreasing from 183±60 V/cm at 0 kbar to 43±13 V/cm at 1 kbar. At 3 kbar the B coefficient is positive which indicates a second-order transition. This observation of a change in the order of the transition is supported by a change in the behavior of the isothermal dielectric constant which has a maximum for E>0 at 0.5 kbar and at E=O at 3 kbar.

This thesis contains brief introductions to the thermodynamics of phase transitions, the phenomenological theory of ferroelectrics, and the structural changes in KH2PO4 produced by the paraelectric to ferroelectric phase transition. Also included is a survey of recent experiments dealing with the order of the KH2PO4 transition at ambient pressure. Details are described of experimental apparatus used to obtain high impedance polarization charge measurement, temperature control to ±2 mK, and hydrostatic pressure generation to 3 kbar with a stability of 10 ppm.

PRESSURE INDUCED TRICRITICAL POINT IN THE FERROELECTRIC PHASE TRANSITION OF POTASSIUM DIHYDROGEN PHOSPHATE

by

ARTHUR BOYD WESTERN, JR.

A thesis submitted in partial fulfillment
of the requirements for the degree

of

DOCTOR OF PHILOSOPHY

in

Physics

Approved:

V. Hugo Schmidt
Chairperson, Graduate Committee

Robert J. Brenna
Head, Major Department

Henry L. Parsons
Graduate Dean

MONTANA STATE UNIVERSITY
Bozeman, Montana

August, 1976

TO JONNEE

ACKNOWLEDGMENTS

The author is grateful for the support of the National Science Foundation under Grant No. DMR74-13220 A01. It is a pleasure to acknowledge the help and guidance of my thesis advisor, V. Hugo Schmidt. I wish to thank him especially for giving me the freedom to develop my own style as a physicist, while always being available for consultation and providing careful criticism of my efforts. I am indebted to Alan G. Baker for construction and maintenance of the pressure system and pressure vessel used in this work and for his aid in taking data at the cost of many nights' sleep. Also thanks to Richard Pollina and Charles Bacon for assistance taking data. A special thank you to Roy Weigand for keeping us supplied with the seven tons of liquid nitrogen used over these years. I have also benefited greatly from the assistance and instruction of electronic technicians Fred Blankenburg and Jay Walker, machinist Cecil Badgley, and Physics Laboratory Supervisor Mark Baldwin, as well as their many work-study students. Thanks too, to Mizuho Kawajiri for translating a paper from Japanese. In addition I am grateful to Dr. Brookeman of Florida State University for supplying the pressure vessel design used in this work. I am grateful to Sprague, Inc. and TRW, Inc. for supplying samples of polystyrene and experimental polypropylene capacitors.

I am indebted in less tangible, but no less important, ways to Kenkichi Okada and Richard Pollina for helpful discussions concerning technical details of the experiment, and to Robert Swenson and Steven Torstveit for theoretical input. In addition, I am greatful to Jack Drumheller for informal conversations which did much to preserve my sanity.

Thanks also to Ann Hewitt for her careful typing of the final manuscript.

Finally, heartfelt thanks to my beloved wife, Jonnee, whose confidence, encouragement, and love have sustained me over these years.

TABLE OF CONTENTS

LIST OF TABLES

LIST OF FIGURES

ABSTRACT

Measurement of the net polarization charge of a KH_2PO_4 crystal as a function of temperature, applied electric field, and hydrostatic pressure indicates the existence of a tricritical point near 2 kbar of pressure. This result is based upon static measurements of the polarization response to applied dc field in a 0.5 K neighborhood of the ferroelectric transition at pressures of 0, 1, and 3 kbar. In each case the paraelectric region is well described by the Landau equation of state, $E=A_0(T-T_0)P+BP^3+CP^5$, to within 0.05 K of the transition temperature. Analysis of the data along lines of constant polarization, which are here called "isopols," indicate that the transition is first-order at 0 and 1 kbar with the critical field decreasing from 183±60 V/cm at 0 kbar to 43±13 V/cm at 1 kbar. At 3 kbar the B coefficient is positive which indicates a second-order transition. This observation of a change in the order of the transition is supported by a change in the behavior of the isothermal dielectric constant which has a maximum for E>0 at 0.5 kbar and at E=0 at 3 kbar.

This thesis contains brief introductions to the thermodynamics of phase transitions, the phenomenological theory of ferroelectrics, and the structural changes in KH_2PO_4 produced by the paraelectric to ferroelectric phase transition. Also included is a survey of recent experiments dealing with the order of the KH_2PO_4 transition at ambient pressure. Details are described of experimental apparatus used to obtain high impedance polarization charge measurement, temperature control to ±2 mK, and hydrostatic pressure generation to 3 kbar with a stability of 10 ppm.

I. BACKGROUND

1. Thermodynamics of Phase Transitions

This section introduces those concepts which are used later in the analysis and discussion of experimental results. A more complete review of the ideas presented below may be found in Introduction to Phase Transitions and Critical Phenomena by Eugene Stanley.[1]

Modern treatments of thermodynamics[1,2] adopt the point of view that there exists a thermodynamic potential, U, whose magnitude depends only upon the values of certain state variables. When the functional dependence of U on these state variables is known and they are specified then the macroscopic state of the system is specified. If these state variables are held fixed by external means all other parameters of the system adjust in such a way as to minimize U. For a dielectric U is a function of the entropy, S, the strains, x, and the polarization, P:

$$U=U(S,x,P), \tag{1}$$

$$dU=TdS-Xdx+EdP,$$

where T is the temperature, X is the stress and E is the external applied field. Some authors refer to U as the internal energy, others the enthalpy. This semantic question, which ultimately depends upon one's choice of the division of energy between the system and its environment, is of no interest here. Callen[2] and Kittel[3] discuss the question at the elementary level for magnetic systems. Leupold derives similar results starting from Maxwell's equations[4] and treats

dielectrics explicitly.[5] It suffices here to say that U so defined is a minimum when S, x, and P are held fixed and is independent of applied field for perfect paraelectrics, i.e. when P is a function of E/T only.

Experimentally it is easier to hold the temperature than the entropy fixed, hence it is useful to define a thermodynamic potential which is an extremum for constant T, x, and P. Such a potential is usually referred to as a free energy. It is related to U via a Legendre transform:

$$F=U-TS, \tag{2}$$
$$F=F(T,x,P),$$
$$dF=-SdT-Xdx+EdP.$$

A second free energy, useful when the applied stress is held constant, is defined

$$H=U-TS+xX=F+xX, \tag{3}$$
$$H=H(T,X,P)$$
$$dH=-SdT+xdX+EdP.$$

Finally, in the experiments to be described later it will be the temperature, stress, and electric field which are held constant. The potential which is a minimum under these conditions is

$$G=U-TS+xX-EP=H-EP, \tag{4}$$
$$G=G(T,X,E),$$
$$dG=-SdT+xdX-PdE.$$

A clear discussion of thermodynamic potentials and Legendre transforms appears in Callen.[2] Leupold has given a complete description of Legendre transforms as applied to ferromagnets[4] and dielectrics.[5]

First partial derivatives of thermodynamic potentials with respect to their proper independent variables yield values for the conjugate variable, e.g. $\partial F/\partial T|_{x,P}=-S$ and $\partial F/\partial P|_{x,T}=E$. Second derivatives yield the so-called response functions, $\partial^2 F/\partial T^2|_{x,P}=TC_{x,P}$ and $\partial^2 F/\partial P^2|_{x,T}= \chi^{-1}{}_{x,T}$ where $C_{x,P}$ is the specific heat at constant strain and polarization, and $\chi^{-1}{}_{x,T}$ is the inverse isothermal clamped dielectric susceptibility.

A phase is a homogeneous system characterized by certain macroscopic parameters. Phase transitions are dramatic in that for small changes in intensive parameters there are large, even divergent, changes in extensive parameters and/or response functions. When ice melts the temperature changes only minutely from below 0 C to just above, yet there is a discontinuous change in volume. In addition the specific heat diverges as quantities of heat are absorbed with negligible change in temperature. Ferroelectrics may show similar anomalies at their transition temperatures including volume change, latent heat, structural change, enormous increase in dielectric constant, and sudden appearance of a large polarization.

One characterization of phase transitions is by the order of the lowest derivative of a thermodynamic potential which suffers a

discontinuity or a divergence at the transition temperature. In the example of melting ice, the first derivative of F with respect to temperature, the entropy, is discontinuous so the transition is first-order. On the other hand, He^4 undergoes a transition from a normal fluid, He I, to a superfluid, He II, with no discontinuity in entropy, but the specific heat diverges. The transition is second-order. The distinction between first- and second-order will be of key importance later.

The concept of a critical point is introduced by once again using water as an example. The projection of the pressure (p), volume (v), temperature (T) surface for water into the pT plane, Fig. 1, shows the coexistence lines between vapor, water, and ice meeting at the triple point. Of particular interest is the coexistence line between vapor and water which terminates in a point known as the critical point (CP). If one crosses this line the density changes discontinuously. But as one crosses the boundary closer to the critical point the discontinuity suffered by the density becomes smaller, until above the CP no discontinuity is observed. By traveling around the CP one can go from gas to liquid continuously with no anomalous behavior.

Letting ρ_ℓ and ρ_g represent the density of the liquid and gas phases respectively, the difference, $\rho_\ell - \rho_g$, goes to zero as the critical temperature is approached from below. Such a quantity

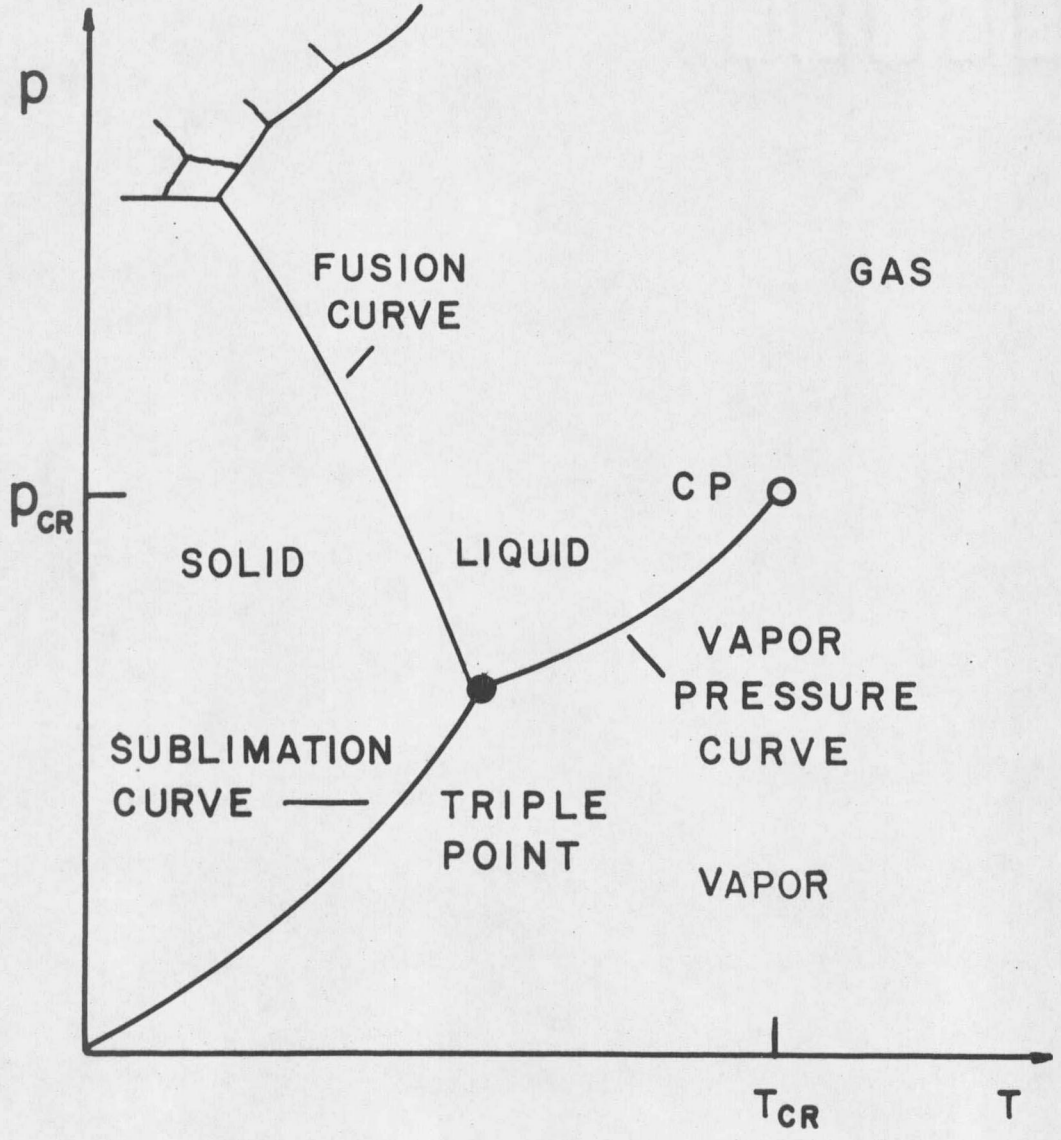

FIG. 1. The projection of the pressure (p), volume (V), and temperature (T) surface for water into the pT plane. The coexistence line between vapor and liquid terminates in a critical point.

which is non-zero below the critical temperature and zero above is a common feature associated with CP's and is known as the order parameter for the transition. In a ferroelectric the spontaneous polarization acts as an order parameter. If the crystal temperature is lowered through the transition temperature, T_c in Fig. 2, there is a jump in the polarization if the transition is first-order. When an electric field is applied to the crystal and the temperature is lowered a similar but smaller jump occurs upon crossing the first order line. Eventually at the critical field, E_{cr} in Fig. 2, the polarization changes smoothly as the temperature is lowered through the transition, but the dielectric constant diverges. At even higher fields the crystal is polarized to such an extent that there is no essential difference between the paraelectric and ferroelectric states near the transition temperature.

Phase transitions may be characterized further by the way in which the order parameter tends to zero as the critical temperature, T_{cr}, is approached. For example in a liquid system one writes

$$\frac{\rho_\ell(T)-\rho_g(T)}{2\rho(T_{cr})} = \frac{\Delta\rho}{2\rho(T_{cr})} = B\left[1-\frac{T}{T_{cr}}\right]^{\beta}[1+\ldots] \qquad (5)$$

to describe the behavior of the order parameter P as T approaches T_{cr} from below. Then β is the critical exponent. In general a critical exponent, λ, for some function f is defined as

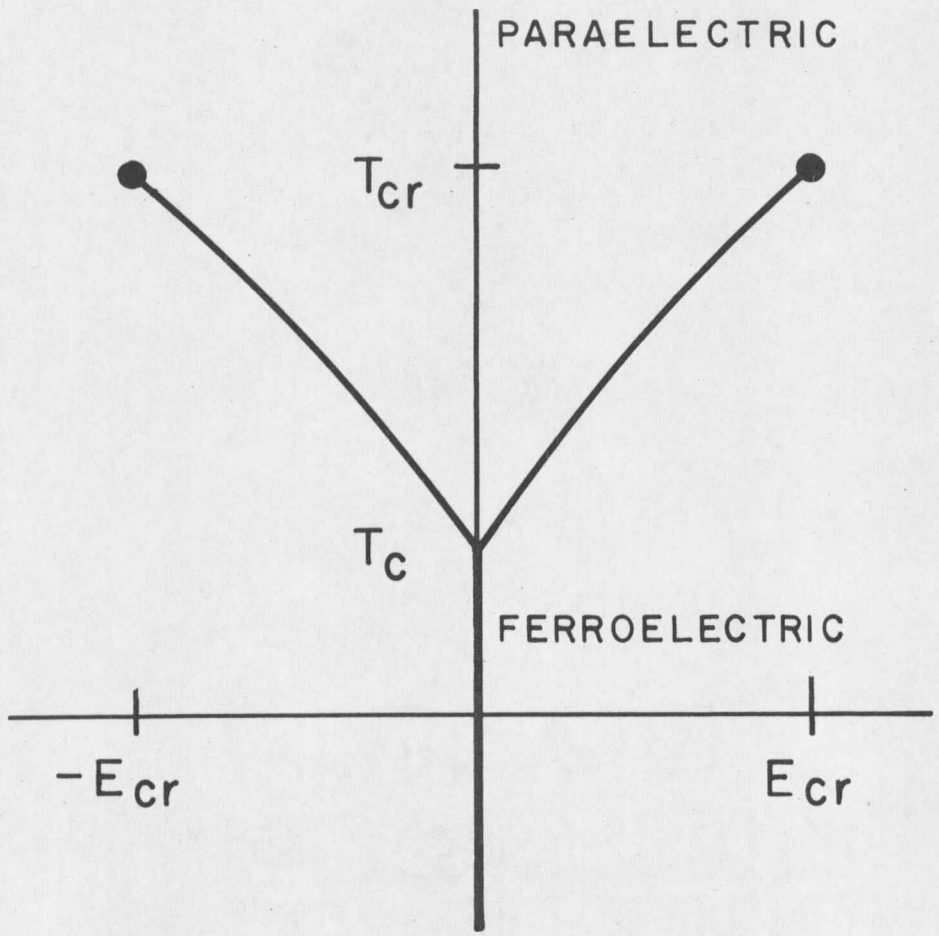

FIG. 2. Phase diagram of KH_2PO_4 in the temperature (T) and electric field (E) plane at zero pressure. The first-order lines terminate at critical points (T_{cr}, $\pm E_{cr}$).

$$\lambda = \lim_{\varepsilon \to 0} \frac{\partial \ln f(\varepsilon)}{\partial \ln \varepsilon} , \tag{6}$$

where ε is $(T/T_{cr})-1$. Such exponents appropriately defined may also characterize divergences at a critical point:

$$\lambda^{j} = \lim_{\varepsilon \to 0} \frac{\partial \ln f^{(j)}(\varepsilon)}{\partial \ln \varepsilon} , \tag{7}$$

where j is the first divergent derivative of the thermodynamic potential f. A list of commonly defined critical exponents is reproduced from Stanley's book[1] in Table I.

The interesting property of critical exponents is that they do not appear to depend upon the details of the physical system but rather upon general features such as the dimensionality and the symmetry of the Hamiltonian.

If one expands a phase diagram with a critical point into a third dimension the critical point may be drawn out into a line of critical points. One possibility, a tricritical point,[6] is shown in Fig. 3. Phase transition lines in Fig. 3 are solid if first-order and dashed if second-order. Note that in the plane of zero ordering field the transition changes from first- to second-order at the tricritical point.

Tricritical points (TCP's) have attracted considerable theoretical interest[6-10] in that they are expected to exhibit different critical exponents than ordinary critical points. Griffiths[7] has proposed

TABLE I. Summary of definitions of critical-point exponents for dielectric systems, after Stanley.[1] Here $\varepsilon=(T/T_{cr})-1$.

Exponent	Definition	Conditions			Quantity
		ε	E	P	
α'	$C_H \sim (-\varepsilon)^{-\alpha'}$	<0	0	0	specific heat at constant E
α	$C_H \sim \varepsilon^{-\alpha}$	>0	0	0	
β	$M \sim (-\varepsilon)^{\beta}$	<0	0	≠0	zero field polarization
γ'	$\chi_T \sim (-\varepsilon)^{-\gamma'}$	<0	0	≠0	zero-field isothermal susceptibility
γ	$\chi_T \sim \varepsilon^{-\gamma}$	>0	0	0	
δ	$H \sim \lvert M\rvert^{\delta}\,\mathrm{sgn}(M)$	0	≠0	≠0	critical isotherm
ν'	$\xi \sim (-\varepsilon)^{-\nu'}$	<0	0	≠0	correlation length
ν	$\xi \sim \varepsilon^{-\nu}$	>0	0	0	
η	$\Gamma(r) \sim \lvert r\rvert^{-(d-2+\eta)}$	0	0	0	pair correlation length

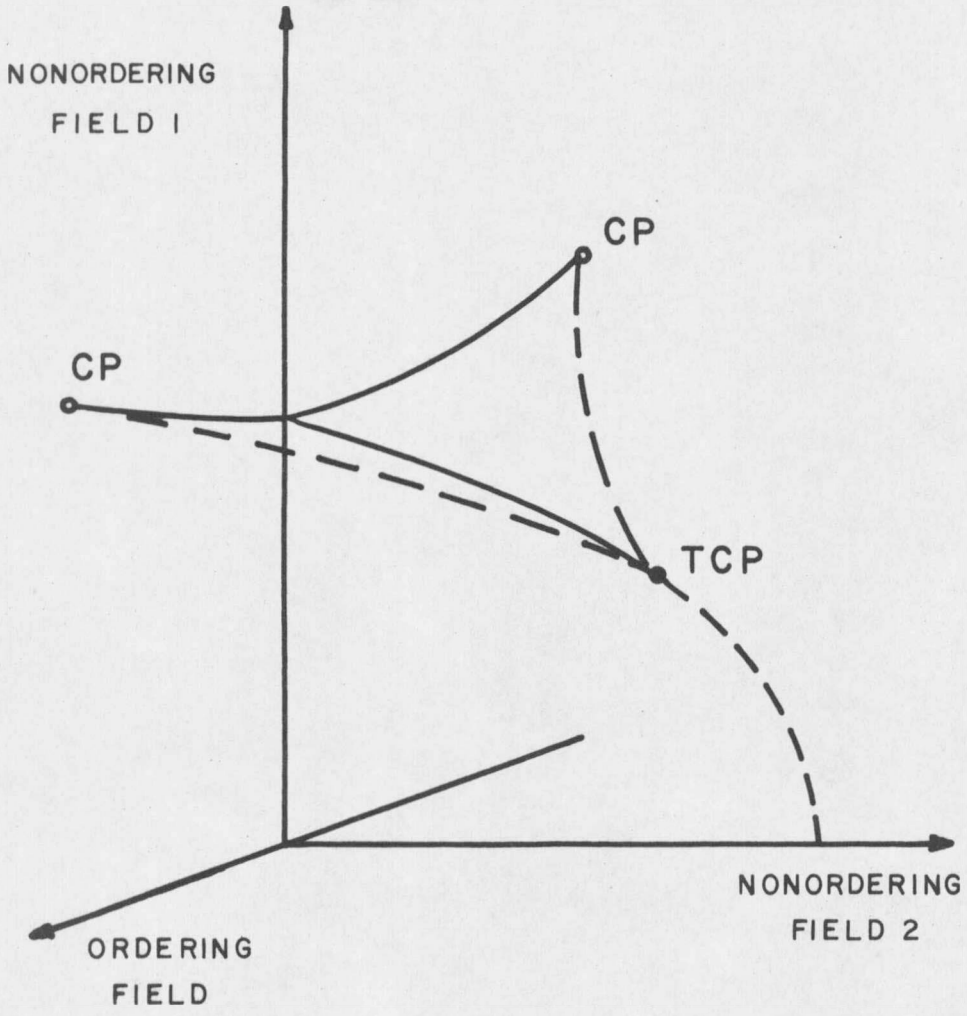

FIG. 3. Topology of a tricritical point. First-order lines are solid, second-order dashed. A tricritical point (TCP) occurs at the intersection of three lines of critical points (CP's).

a notation for tricritical exponents in the zero ordering field plane. Exponents are subscripted t if the TCP is considered one of a series of critical points, i.e., part of the dashed line in the zero ordering field plane of Fig. 3. The subscript u is used when the TCP is considered as the terminus of a first order line in analogy to an "ordinary" critical point. Clearly if one does not restrict one's self to the zero ordering field plane it is possible to define a large number of different kinds of exponents as the TCP is approached along a variety of paths singled out by the topology of Fig. 3. The important point to keep clear is that every exponent involves a path, and that path must be clearly stated before the exponent has meaning.

Experimentally TCP's have been shown to exist in a number of systems: He^3-He^4 mixtures,[11] magnetic systems (DyAl garnet,[12] $FeCl_2$[13]), the structural transition in NH_4Cl[14] and in the ferroelectric SbSI.[15] The first three of these suffer from the drawback that the TCP can be investigated only in the zero ordering field plane. The wing structure (see Fig. 3) is inaccessible as the fields which would have to be applied are impossible to produce experimentally. SbSI suffers from other difficulties: it grows in long slender crystals inappropriate for dielectric studies, and it tends to decompose by the evaporation of iodine.

The impetus for this present work was the conjecture by V. H. Schmidt[16] that KH_2PO_4 (KDP) would have a TCP for which the ordering

field in its phase diagram is experimentally available. The existence of such a TCP is of considerable importance as it would represent an opportunity to study a TCP in its entire phase space. Moreover, crystals of high quality are commercially available in virtually any size, and, although hygroscopic, they are otherwise quite stable.

2. Description of KH_2PO_4

Potassium Dihydrogen Phosphate (KDP) is the archetype of a class of isomorphous hydrogen-bonded ferroelectrics. Since the first report of its ferroelectric properties in 1935[17] it has been the subject of literally hundreds of papers. Only a few of its most fundamental properties are outlined here. A more complete introduction to work prior to 1960 may be found in Jona and Shirane.[18] More recent results and an extensive review of existing literature may be found in "Ferroelectric Hydrogen-Bonded Systems" by V. H. Schmidt.[19]

KDP is a ferroelectric; that is, it develops a spontaneous dipole moment below its transition temperature and that polarization can be reversed by application of an external electric field. Its structure is shown in Fig. 4 and described by Jona and Shirane:[18]

> Each phosphorus atom is surrounded by four oxygen atoms at the corners of a tetrahedron which is almost regular (being compressed by approximately 2% along the c axis). These PO_4 groups, together with the potassium atoms, build up a structure

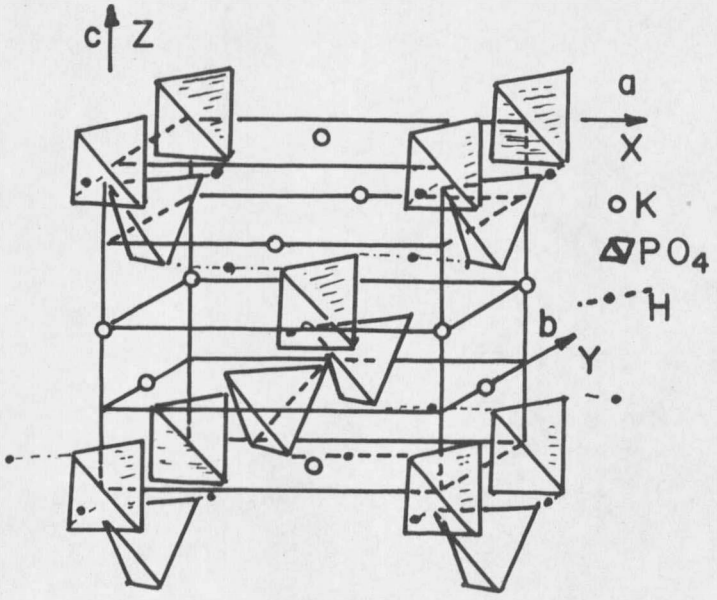

FIG. 4. Structure of KH_2PO_4, after West.[22]

> in such a way that K and P atoms alternate with each other at a distance of c/2 in the direction of the c axis. Every PO_4 is linked to four other PO_4 groups, spaced c/4 apart along c, by hydrogen bonds. Thus the linkage is such that there is a hydrogen bond between one "upper" oxygen of one PO_4 group and one "lower" oxygen of the neighboring PO_4 group, and each hydrogen bond lies nearly perpendicular to the c axis.

Neutron diffraction data[20] reveal that the hydrogens are located in one of two off-center positions within the hydrogen bond. Generally in the four hydrogen bonds associated with a PO_4 group, two of the hydrogens occupy off-center positions close to the PO_4 group and the other two occupy far positions (close to the neighboring PO_4 groups). It may happen that three hydrogens are close or far. These Takagi[21] configurations are statistically less frequent but are important for the crystal dynamics. Still rarer, and of no obvious importance, are H_4PO_4 and PO_4 groups. The remarkable feature of the transition is that, although the two close hydrogens are randomly located amongst the four bonds above the transition, below the transition the close hydrogens are always found at the top of the PO_4 tetrahedron (or bottom for the opposite polarization). Thus the transition is order-disorder with respect to the position of the hydrogen atoms.[18]

As pointed out in the description of the crystal structure, the hydrogen bonds are perpendicular to the c axis along which the

polarization is directed. Thus it is not the hydrogen ordering which is directly responsible for the production of the dipole moment of the crystal. Rather it is the displacement of the P and K ions along the c axis which accompanies the hydrogen ordering which is responsible for the net charge displacement and the dipole moment. Thus the transition is a displacive one with respect to the movement of the K, P, and O ions.[18]

In addition, the crystal polarization is accompanied by a shear strain perpendicular to the c axis. This shear is directly proportional to the polarization whether it is field-induced above the transition or spontaneous below, and with the same (slightly temperature dependent) constant of proportionality.[18]

The hydrogen ordering has been treated as a two-level problem by considering only the slightly separated ground state energies of the double-well potential hydrogen bond, and then casting the problem in terms of two-by-two Pauli matrices, as can be done for any two-level problem. The hydrogen atom dynamics are then described as a pseudo-spin wave.[23] Thus, in the parlance of fundamental excitations, one has a pseudo-spin wave interacting with a transverse optical phonon (associated with the K and P motion) and with an acoustic phonon (associated with the x-y shear). This rich variety of phenomena is one of the reasons why KDP has attracted so much theoretical and experimental interest over the past forty years.

Moreover, it appears that this crystal is to become of even further interest owing to the existence of a tricritical point in its phase diagram. In some sense microscopic descriptions of the KDP transition foreshadowed this result. In the statistical theory of Slater[24] and Takagi[21] as developed by Silsbee, Uehling, and Schmidt (SUS),[25] and in the theory of Blinc and Svetina[23] which takes proton tunneling into account, the transition is first-order or second-order depending upon the values of a few parameters describing the microscopic interactions. Since the transition (as will be documented later) is just barely first-order at atmospheric pressure, it is perhaps not surprising that small distortions of the crystal by applied pressure might tip the scales in favor of a second-order transition thus producing the TCP. Since much is known regarding KDP's structure, it should prove fertile ground for theorists who would explain the associated critical phenomena.

3. Introduction to Landau-Ginzburg-Devonshire Theory

The experimental results presented in Chapter III are analyzed primarily in terms of the phenomenological theory of Landau.[26] A brief introduction is given here. For further details the reader is referred to Landau,[26] Ginzburg,[27] and Devonshire.[28] A complete account of the phenomenological theory of ferroelectrics may be found in Grindlay's book[29] as well as that of Fatuzzo and Merz.[30]

The central point of the Landau-Ginzburg-Devonshire theory is that the free energy H(T,X,P) may be expanded in a power series in the stress and the polarization,

$$H(T,X,P)=H(T,0,0)+\tfrac{1}{2}\sum_{ij}\gamma_{ij}P_iP_j+\tfrac{1}{4}\sum_{ijk\ell}\xi_{ijk\ell}P_iP_jP_kP_\ell \qquad (8)$$
$$+\tfrac{1}{6}\sum_{\substack{ijk\\ \ell mn}}\zeta_{ijk\ell mn}P_iP_jP_kP_\ell P_mP_n+\tfrac{1}{2}\sum_{ijk\ell}S_{ijk\ell}X_{ij}X_{k\ell}+\sum_{ijk}a_{ijk}X_{ij}P_k$$
$$+\tfrac{1}{2}\sum_{ij\ell m}q_{ij\ell m}X_{ij}P_\ell P_m.$$

The $s_{ijk\ell}$ coefficients are tensors of elastic compliances, a_{ijk} are piezoelastic tensors, and $q_{ijk\ell}$ are electrostrictive tensors. Higher-order terms may of course be included, but the ones shown are sufficient to describe all known ferroelectric phenomena.[29] Odd powers of the polarization have been omitted as the crystal symmetry demands.[31] If one restricts consideration to KDP, a uniaxial ferroelectric, under hydrostatic pressure the equation greatly simplifies:

$$H(T,X,P)=H(T,0,0)+\tfrac{1}{2}A'P^2+\tfrac{1}{4}BP^4+\tfrac{1}{6}CP^6+\tfrac{1}{2}SX^2+\tfrac{1}{2}QXP^2, \qquad (9)$$

where the piezoelectric term is also omitted as KDP has no linear piezoelastic coupling in the high temperature phase due to symmetry.[18] A further simplification can be made if one suppresses the display of the purely elastic energy, $\frac{1}{2}SX^2$, and the electrostrictive term, $\frac{1}{2}QXP^2$. The free energy is then

$$H=\tfrac{1}{2}AP^2+\tfrac{1}{4}BP^4+\tfrac{1}{6}CP^6 \qquad (10)$$

For a fixed pressure this free energy function describes the thermodynamic state of the crystal. The coefficients A, B, and C may be functions of temperature and/or pressure. In particular, the inverse isothermal dielectric constant decreases linearly with temperature in the paraelectric phase (Curie-Weiss law) extrapolating to zero at T_o, the Curie-Weiss temperature. This behavior can be described in the free energy by writing $A=A_o(T-T_o)$, so that

$$H=\tfrac{1}{2}A_o(T-T_o)P^2+\tfrac{1}{4}BP^4+\tfrac{1}{6}CP^6. \qquad (11)$$

The point of view taken in this thesis is to describe the temperature and pressure dependences of the parameters A_o,T_o,B, and C, suppressing explicit terms depending upon the pressure in the free energy. This seems desirable in an experimental paper as there remains lack of agreement amongst theoretical treatments of the KDP transition. For example, Hegenbarth and Ullwer[32] lump the electrostrictive term with $A_o(T-T_o)P^2$ and show that the electrostriction accounts for the lowering of the transition temperature with pressure. On the other hand Vaks and Sidnenko[33] take this same electrostrictive term, argue that strain is proportional to P^2, and hence lump it with the BP^4 term and report that it is responsible for the first-order nature of the transition. While both treatments may be correct, the experiments described here are not sufficient to separate electrostrictive energy from other pressure effects, let alone separate it

into a quadratic and a quartic part. Hence explicit pressure dependence due to separate mechanisms is suppressed.

Experimentally it is the external field, E, which is held constant and thus

$$G(T,X,E)=H(T,X,P)-EP \tag{12}$$

is the appropriate thermodynamic potential to minimize. For E=0, however, there is no difference between H and G. Thus for a crystal whose faces are shorted together one may minimize H at fixed T, p, and E=0 with respect to P to find the equilibrium state of the system. Fig. 5 shows H vs. the parameter P for various temperatures and a positive and negative B. If the crystal passes only through absolutely stable thermodynamic states, the value of P corresponding to the minimum of H is actually obtained.

At the transition temperature, T_c, Fig. 5a shows that three distinct values of the polarization minimize the free energy, so these polarizations coexist. Slightly above T_c the polarization must be zero, while slightly below it must jump to a non-zero value. This jump in polarization at the transition temperature is a characteristic of a first-order transition. The two positive hills in the free energy of Fig. 5a are due to the negativity of B. In Fig. 5b where B is assumed positive no such humps appear; P changes rapidly with temperature just below T_c, but it does not jump discontinuously.

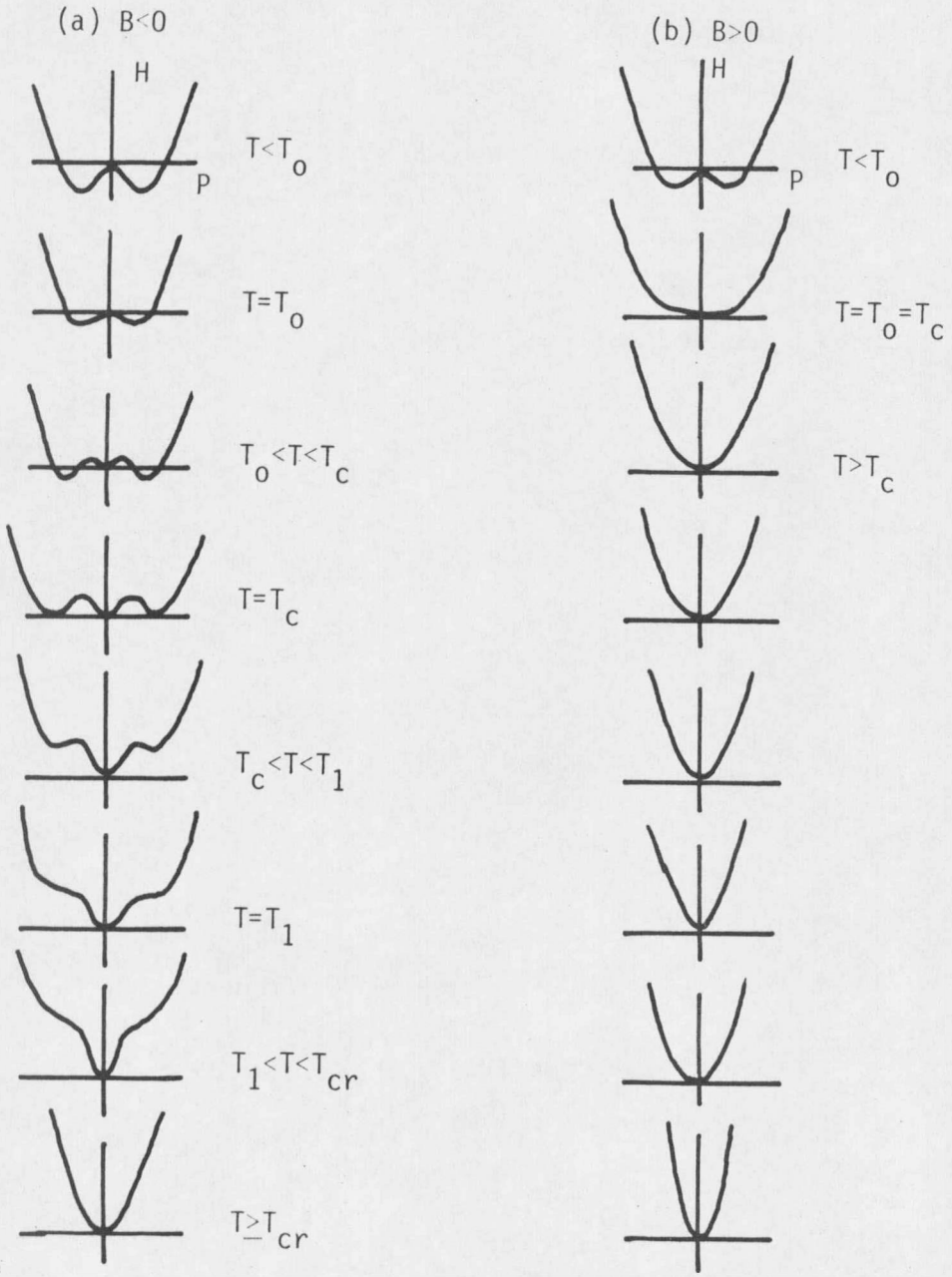

FIG. 5. $H=\frac{1}{2}A_o(T-T_o)P^2+\frac{1}{4}BP^4+\frac{1}{6}CP^6$ vs. P for (a) B<0 and (b) B>0. T_o is the Curie-Weiss temperature, T_c the Curie temperature, T_1 the metastability limit, and T_{cr} the critical temperature.

It can be shown easily that the inverse dielectric constant (second derivative of H with respect to P) jumps discontinuously at T_c if B is negative (first-order transition), but is continuous with a discontinuous slope at T_c if B is positive (second-order transition). Graphs of these two ideal types of behavior are shown in Fig. 6.

If metastable thermodynamic states are allowed, a first-order transition may exhibit thermal hysteresis. The picture here is that the crystal may remain in a local minimum well of the free energy even when the bottom of that well has higher energy than the absolute minimum. That is, if the crystal is polarized to $P \neq 0$ at $T<T_c$ and the temperature raised, the possibility exists that the crystal will remain polarized for $T>T_c$ if the thermal fluctuations are not sufficient to allow the crystal to "jump the hill" separating it from the absolute minimum at P=0. The reverse situation may arise when the temperature is lowered. No such possibility exists when the transition is second-order. The maximum possible extent of the hysteresis is of course when the metastable minimum disappears (becomes locally unstable). The high and low temperature limits for hysteresis are called T_1 and T_o following Fatuzzo and Merz.[30]

If a non-zero electric field is applied to the crystal the full potential G(T,p,E) must be used. Although G(T,p,E) is not a proper thermodynamic function of the polarization, it is still instructive to graph its parametric dependence on P. This is shown in Fig. 7

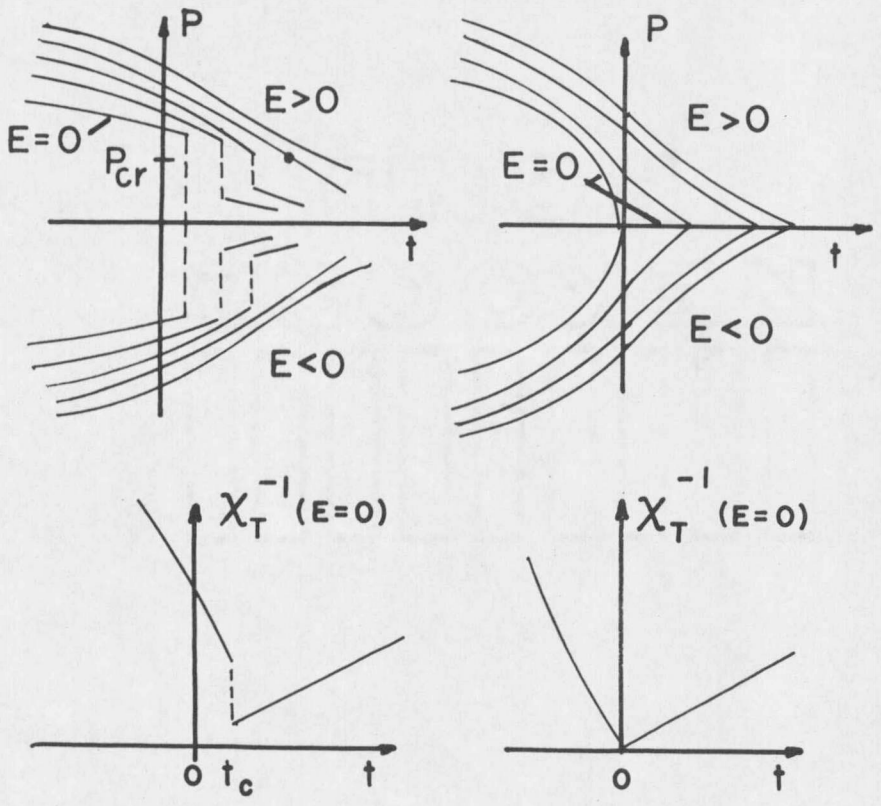

(a) B<0 (b) B>0

FIG. 6. Idealized behavior of the polarization and inverse isothermal susceptibility for (a) first- and (b) second-order transitions as predicted from the free energy $H=\frac{1}{2}A_0(T-T_0)P^2+\frac{1}{4}BP^4+\frac{1}{6}CP^6$. The order of the transition depends upon the sign of B. Here $t=(T/T_0)-1$. (After Grindlay[29])

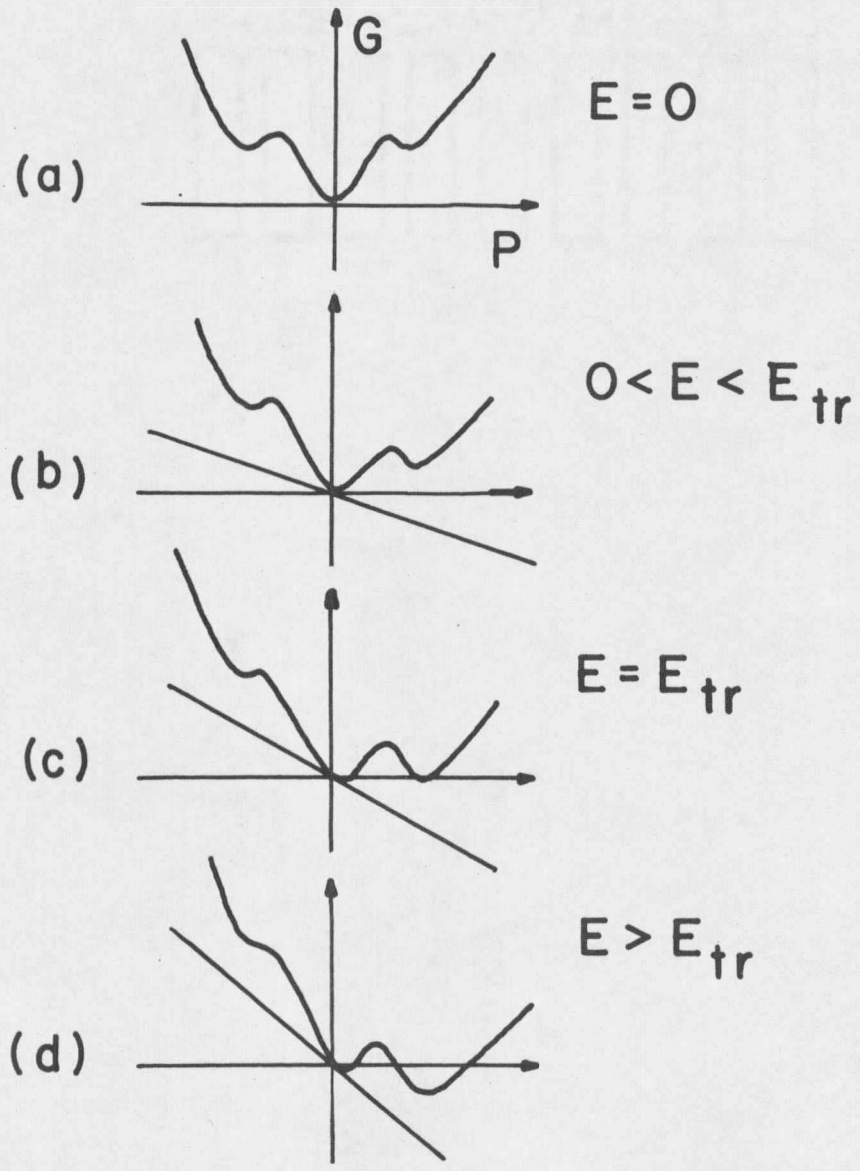

FIG. 7. The free energy G=H-EP for four bias fields at constant T, $T_c<T<T_{cr}$.

for various values of E at a fixed temperature T, $T_c<T<T_{cr}$. A first-order transition may now be induced by the application of a sufficiently large electric field. For fields less than the transition field, E_{tr}, the minimum of G is at P=0; for $E>E_{tr}$ the minimum is at P>0 and the crystal polarization jumps discontinuously to this value (perhaps with hysteresis). This construction is completely equivalent to the bi-tangent construction to the free energy H which may be more familiar to some readers.

If the temperature is raised above T_{cr} then the two minima in Fig. 7c coalesce into one and there can be no further first-order transition. The temperature, T_{cr}, and field, E_{cr}, where this occurs are the coordinates of the critical point at the terminus of the first-order line in the temperature-electric field plane. This point has the properties of a second-order transition.

One can find exact expressions for the various special temperatures and other quantities of interest directly from the expression for the free energy. One finds T_c by requiring H=0, P≠0 have a single positive root. The temperature T_{cr} is where the two points of inflection of H merge into one, hence $d^2H/dP^2=0$ has only one positive root. It is then a simple matter of algebra to solve for the other quantities of interest. The results are:

$$T_c - T_o = 3B^2/16A_oC$$
$$T_{cr} - T_o = 9B^2/20A_oC \qquad (13)$$
$$E_{cr} = (2(-B/5)^5/(C/3)^3)^{1/2}$$
$$\Delta P_{spon}(T_c) = (-3B/4C)^{1/2}$$

where $\Delta P_{spon}(T_c)$ is the jump in polarization occurring at T_c.

Standard mean field exponents may be derived by considering the dependence of such quantities on $T-T_c$. The results are:[1]

$\alpha' = \alpha = 0$, $\beta = \frac{1}{2}$, $\gamma' = \gamma = 1$, $\delta = 3$.

In the context of the mean-field Landau-Ginzburg-Devonshire free energy expression, the condition for a tricritical point is that B change continuously from positive to negative as a function of some parameter. The TCP occurs when B=0. In Chapter III results are presented which indicate that a TCP does exist in KDP at high pressure where the coefficient B is driven to zero.

4. Review of Recent Relevant Experiments

Prior to 1969 the transition in KDP was generally thought to be second-order.[18] Recent results indicate that it is in fact first-order but quite close to being second-order. This opinion is now supported by a number of experiments done in various countries. In Russia, Strukov[34] exploited KDP's large electrocaloric effect and measured the temperature change produced by the sudden application of an electric field. Gladkii and Sidnenko[35] measured the polarization

vs. temperature of the crystal in various electric fields. Garber and Smolenko[36] made painstaking dilatometric measurements of the crystal dimensions near the transition. Vallade and coworkers[37] in France have measured the polarization vs. temperature dependence of KDP by optical birefringence. Okada and Sugie´ and others in Japan have studied the KDP transition extensively. They have reported on the temperature sweep rate dependence of the thermal hysteresis,[38] the difference between the adiabatic and isothermal dielectric constant,[39] and hysteresis loop measurements of the polarization vs. applied field at constant temperature.[40] In this country, Reese has studied the transition in a number of carefully done calorimetric experiments.[41,42] The most recent results of all of these groups are in fair agreement as to the coordinates of the critical point at the end of the first-order line (200-300 V/cm) and the fact that KDP obeys the phenomenological theory of Landau to within at least 0.1 K of the transition temperature.

There are, however, three experiments described in the literature which yielded markedly different results. The first of these is an x-ray dilatometric study by Kobayashi et al.[43] who found a critical field of 8500 V/cm, much higher than the critical fields of 200-300 V/cm found in the experiments described above. Matsuda and Abe[44] calculate the B coefficient in the Landau free energy from measurements of the third harmonic of a 1 kHz ac electric field applied

to the crystal. Their value is two orders of magnitude larger (in absolute value) than reported in the papers cited earlier. Finally, Eberhard and Horn[45] (EH) studied the thermal hysteresis of the transition at various applied fields and concluded E_{cr}=6500 V/cm. There is reason to believe this value should be revised downward closer to 300 V/cm.[46] EH have recently revised that result to 1200 V/cm.[47]

The latest published results of all of these workers is displayed in Table II along with published[48] and unpublished results of the Montana State University group.

Far less work has been done on the KDP transition at elevated pressures. Samara[49] evaluated the change of T_c and A_o with pressure using a small-signal ac field to measure the dielectric response of the crystal. He found dT_c/dp=-4.6 K/kbar and $(dA_o/dp)/A_o$=-7x10^{-3} kbar^{-1} at pressures to about 7 kbar. The transition temperature then decreased rapidly to 0 K at 17 kbar. The transition temperature appeared to approach 0 K with an infinite slope.

Hegenbarth and Üllwer[32] (HU) performed essentially the same experiment up to 1.6 kbar and found the initial decrease of T_c with pressure to be -5.6 K/kbar. HU attributed the change in T_c to the electrostrictive term in the free energy and found reasonable agreement with the required magnitude of the appropriate elastic constants.

TABLE II. Summary of recent published values of the parameters in the free energy $H=\frac{1}{2}A_o(T-T_o)P^2+\frac{1}{4}BP^4+\frac{1}{6}CP^6+\frac{1}{8}DP^8$ and derived coordinates of the critical point at ambient pressure.

	A_o, 10^{-3} esu	B, 10^{-11} esu	C, 10^{-19} esu	D, 10^{-27} esu	E_{cr}, V/cm	$T_{cr}-T_o$, K
Strukov[34]	3.9	-1.9	6.3	0	120	0.07
Sidnenko[35]	3.8±0.1	-3.0±0.8	6.5±1.1	0	370	0.16
	3.8±0.1	-0.5±0.3	0	3.8±0.4	87	0.036
Vallade[37]	3.9	-0.54±0.05	0	2.85±0.10	124	0.046
	3.9	-1.85±0.25	3.3±0.5	0.87±0.5	280	0.11
Okada[40]	4.2±0.1	-1.9±0.1	5.4±0.4	0	160	0.07
Benepe[42]	(3.81)	-0.44	0	2.96	84	0.055
Kobayashi[43]	(3.86)	-11.9	11.0	0	8500	1.50
Matsuda[44]	---	-110.	---	---	---	---
Eberhard[45]	(7.3)[46]	-2.2	0.6	0	6500	0.51
MSU						
Sample 1[48]	4.3±0.2	2.35±0.4	5.91±1.5	0	232±70	0.10±0.03
Sample 2	4.0±0.2	1.48±0.2	3.1±0.4	0	186±60	0.08±0.03

In neither of the above two experiments was the temperature resolution sufficient to monitor the order of the transition.

The purpose of the experiments described in this thesis was to (1) resolve the controversy regarding the coordinates of the critical point at zero pressure, (2) to monitor those coordinates with increasing pressure, and (3) determine if the transition becomes second-order at high pressure, thus indicating the existence of a tricritical point in the phase diagram of KDP.

II. EXPERIMENTAL

The accomplishment of the goals set forth at the end of Chapter I required considerable care in the measurement of polarization, electric field, temperature, and pressure. Results of other workers which indicate the precision necessary are reviewed below. Then follow descriptions of the actual hardware used to obtain that precision.

1. Experimental Requirements

One measure of the first-order nature of a transition is the difference between T_o and T_c. Here T_o is that temperature where the inverse dielectric constant in the paraelectric region extrapolates to zero, and T_c is the actual transition temperature. For KDP, T_o-T_c values from 0.01 K to 0.63 K appear in the literature.[34-44] Clearly if the T gap was as small as a few hundredths of a degree, temperature resolution on the order of millidegrees is called for. Moreover, Okada[38], and Garber and Smolenko[36] have shown that temperature drift rates as small as 0.1 K/hr would be too fast to exhibit equilibrium properties of the crystal. Thus the temperature would have to be stable to millidegree accuracy.

In earlier pressure studies Samara,[49] and Hegenbarth and Ullwer[32] found that the transition temperature of KDP changed on the order of -5 K/kbar. Thus pressure stability of ±0.25 bar would be necessary to match temperature stability of ±2.5 mK. This is 10 ppm at 2.5 kbar,

a stringent requirement on a small volume system. This difficulty is compounded by the use of helium gas as a pressure medium which was necessary in order to maintain hydrostatic pressure up to 7 kbar at temperatures as low as 70 K.

For reasons discussed in the beginning of Chapter III, static dielectric measurements were necessary to determine the order of the transition. To cover any reasonable temperature range (e.g. 0.5 K) in steps of, say, a few hundredths of a degree, a high impedance electrometer was necessary to measure the polarization charge without draining that charge to ground excessively over a period of days. In addition this charge would have to be stored on a large low-leakage capacitor. An effective RC time constant of 8×10^6 sec is the best so far obtained. This results in a leakage of 1.1% in 24 hr. Guarded circuitry and Teflon insulation were used to insure that leakage currents to ground did not deteriorate this value.

2. Sample Preparation

Sample No. 1 was obtained from Interactive Radiation, Inc.[50] in May of 1974 and stored in a small vial with calcium sulfate desiccant until June of 1975. Crystal dimensions were 1x1x0.2 cm, the large faces being perpendicular to the ferroelectric c axis. Gold electrodes were evaporated onto the large faces in a vacuum of 10^{-4} torr. The evaporator consisted of a tungsten filament wound

with gold wire. The filament was heated white hot with a large current fed into the vacuum chamber *via* spark plug feedthroughs. On one large face of the crystal a circle of 32 gauge wire was used as a mask during evaporation to create a guard ring configuration. The average diameter of the nearly circular center electrode was 0.671±0.004 cm and the unplated annular guard ring width was 0.0377±0.007 cm. This yielded an effective center electrode area of 0.40±0.02 cm^2.

The temperature of sample No. 1 was lowered to the transition region five times between July and December of 1975. This took about three hours on each occasion. No measurements were taken on the first occasion due to cryostat problems. On the second trial the small signal (0.05 V/cm) ac dielectric constant was measured at 1 kHz. A rounded transition was observed as shown in Fig. 8. The maximum dielectric constant was 10 000. This run was then terminated. Upon inspecting the crystal it was found that each of the four corners had broken off (see Fig. 8). It was then discovered that the compression spring of the spring-loaded sample holder was fully compressed causing considerable pressure at the center of the crystal from the approximately 1 mm^2 central contact of the crystal holder. This condition was relieved and the crystal held as lightly as the holder and the available manual dexterity would allow. Run No. 3 was aborted when the ac measurements indicated a broken lead wire.

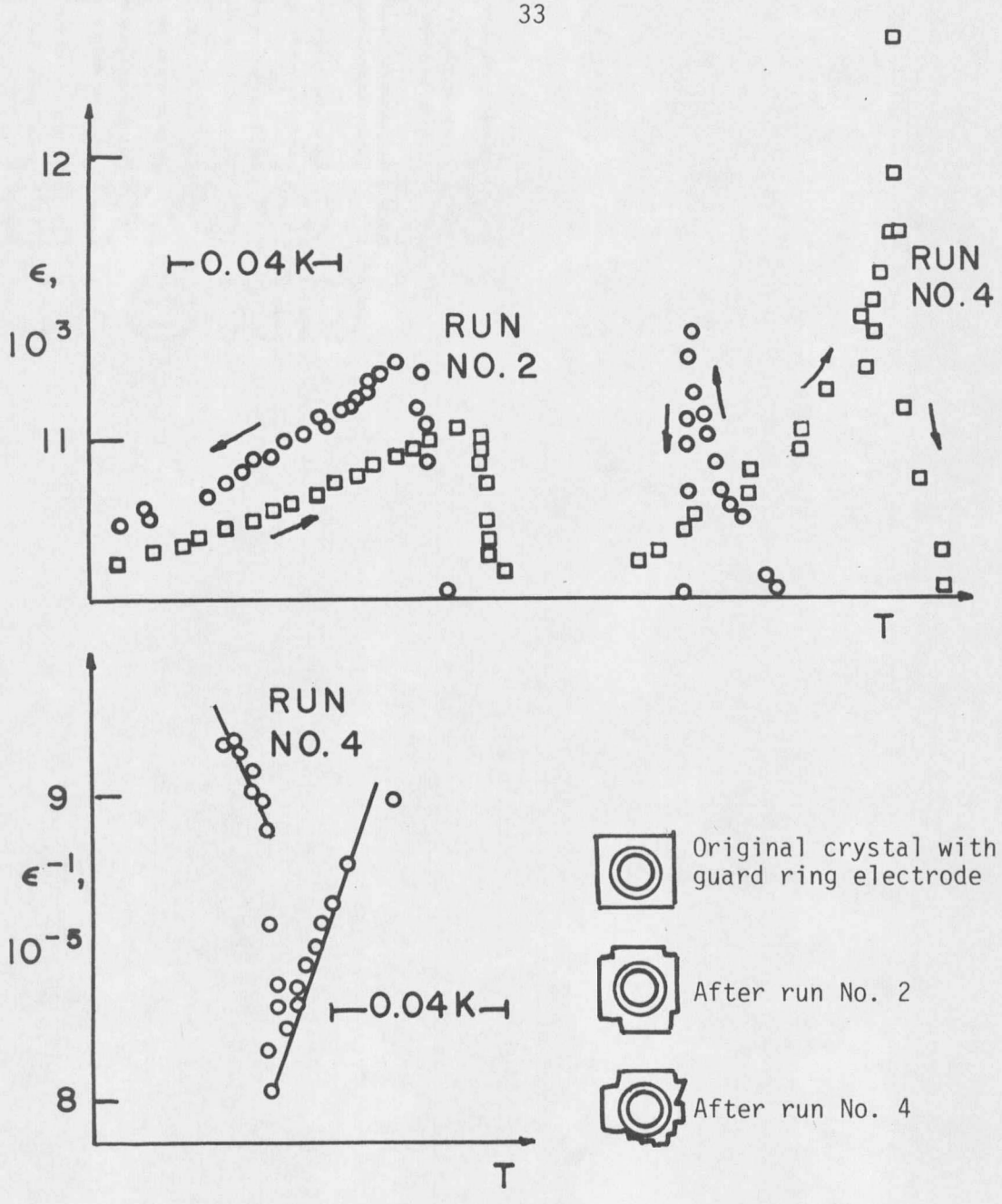

FIG. 8. A visual history of sample No. 1.

On run No. 4 the ac dielectric constant was higher (ε_{max}=12 500) and the transition was not rounded within the available resolution (see Fig. 8). A graph of ε^{-1} is especially interesting for this crystal as it indicates a downward jump discontinuity in ε at the transition followed by a continuous decrease in ε below T_c. This type of behavior is predicted by Landau theory but is not the usual behavior of KDP; in fact we have seen it in no other crystals. Run No. 4 lasted from 10 September to 8 November during which time the crystal remained near the transition temperature, although it was actually brought through the transition fewer than a dozen times. Run No. 4 was terminated when a buildup of frost around the dewar top put sufficient pressure on the back-to-air valve to break the solder joint and destroy the vacuum.

Routine inspection showed that sample No. 1 was badly cracked around the outside of the guard ring; nearly a third of the outer area had broken away. This is likely due to the spring pressure of the guard ring contact of the crystal holder. The center electrode area appeared to be free of cracks. A subsequent attempt to take further data on sample No. 1 led to inconsistencies with previous data which could not be reconciled by minor area corrections.

Sample No. 2 was obtained from Cleveland Crystals, Inc.[51] in May of 1974 and stored in a small vial with calcium sulfate desiccant until 13 January 1976. Crystal dimensions were 1x1x0.2 cm, the large

faces being perpendicular to the ferroelectric c axis. Chrome-gold electrodes had been evaporated on the surface by the supplier. No guard ring was used. The 0.0025 in. diameter solid copperweld center wires of Type A Ultraminiature Coaxial Cable[52] were attached to the evaporated electrode faces by means of silver paint[53] applied as small (2 mm^2) dots on either side. Five coats were used in an effort to increase the strength of the bond as these lead wires were the sole support for the crystal. Thus the only stress on the freely hanging crystal was its own weight. The crystal face area was 0.995 ± 0.02 cm^2; its thickness was 0.1962 ± 0.0002 cm.

Sample No. 2 was pressurized with He gas, then vented to ambient pressure a number of times at room temperature in order to flush the pressure vessel of moisture and air: four cycles to 500 psi, three cycles to 1000 psi, two cycles to 1500 psi, and once to 15 000 psi. The sample temperature was then lowered to near T_c in a period of about five hours.

The small signal (0.05 V/cm) ac dielectric constant (ε) was measured at 1 kHz. For 0.3 K above T_c a straight line was obtained for ε^{-1} *vs.* T in accordance with the Curie-Weiss law. A slight decrease in ε occurred 40 mK above T_o, then the dielectric constant rose to the incredibly high value of 360 000 after which it stayed flat for at least 0.2 K above T_o. This high dielectric constant was checked carefully below T_o with even smaller ac field (0.005 V/cm)

and found to be at least 300 000. Fig. 9 shows ε^{-1} vs. T for sample No. 2. The crystal remained near T_c at ambient pressure until 4 March when it was pressurized to 1 kbar. The crystal then remained near the 1 kbar transition temperature until 4 May when it was returned to ambient pressure and raised to room temperature.

The crystal, upon inspection, showed no visible deterioration. The crystal was again lowered to the transition temperature, this time over a period of four days. Electrical measurements at 1 bar were made, and the crystal was then pressurized to three kbar. The temperature was then lowered 15 K in about twelve hours. The crystal remained near the 3 kbar transition until 19 June. The crystal was then heated five degrees, and the pressure lowered to 2 kbar. On 30 June the crystal was raised to room temperature, and the system was vented to ambient pressure over a period of days.

3. Temperature Control

The cryostat used to control the pressure vessel temperature consists of three concentric cylinders with the 0.25 in. high-pressure tubing acting as the central connecting axis. A schematic drawing of the entire assembly is shown in Fig. 10. The innermost piece is the pressure vessel (PV) itself at the termination of the pressure tubing. Surrounding the PV is a copper can 3 in. in diameter and 12 in. long. The top of the can is attached to the pressure

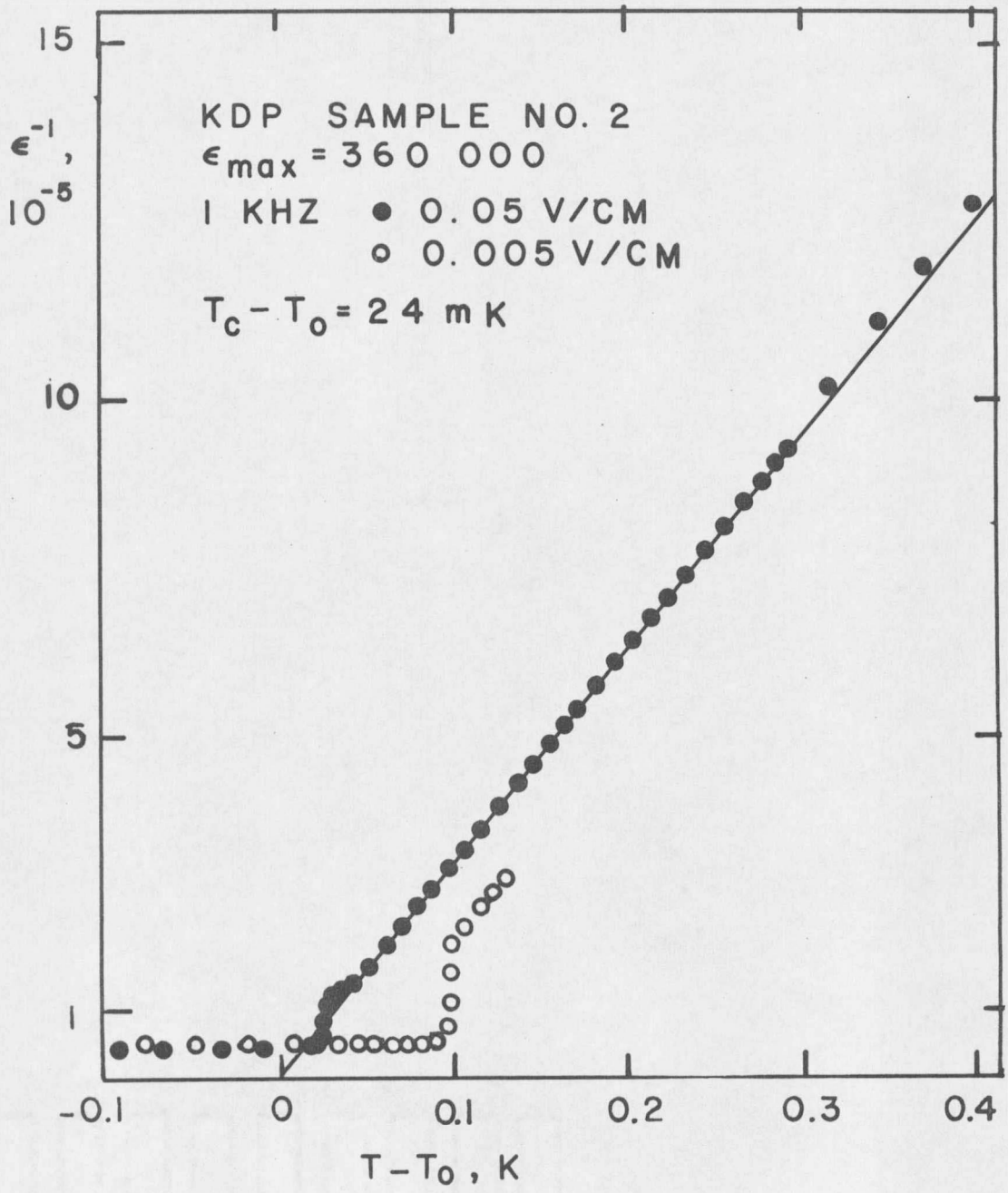

FIG. 9. Inverse dielectric constant vs. temperature for sample No. 2. Hysteresis is instrumental.

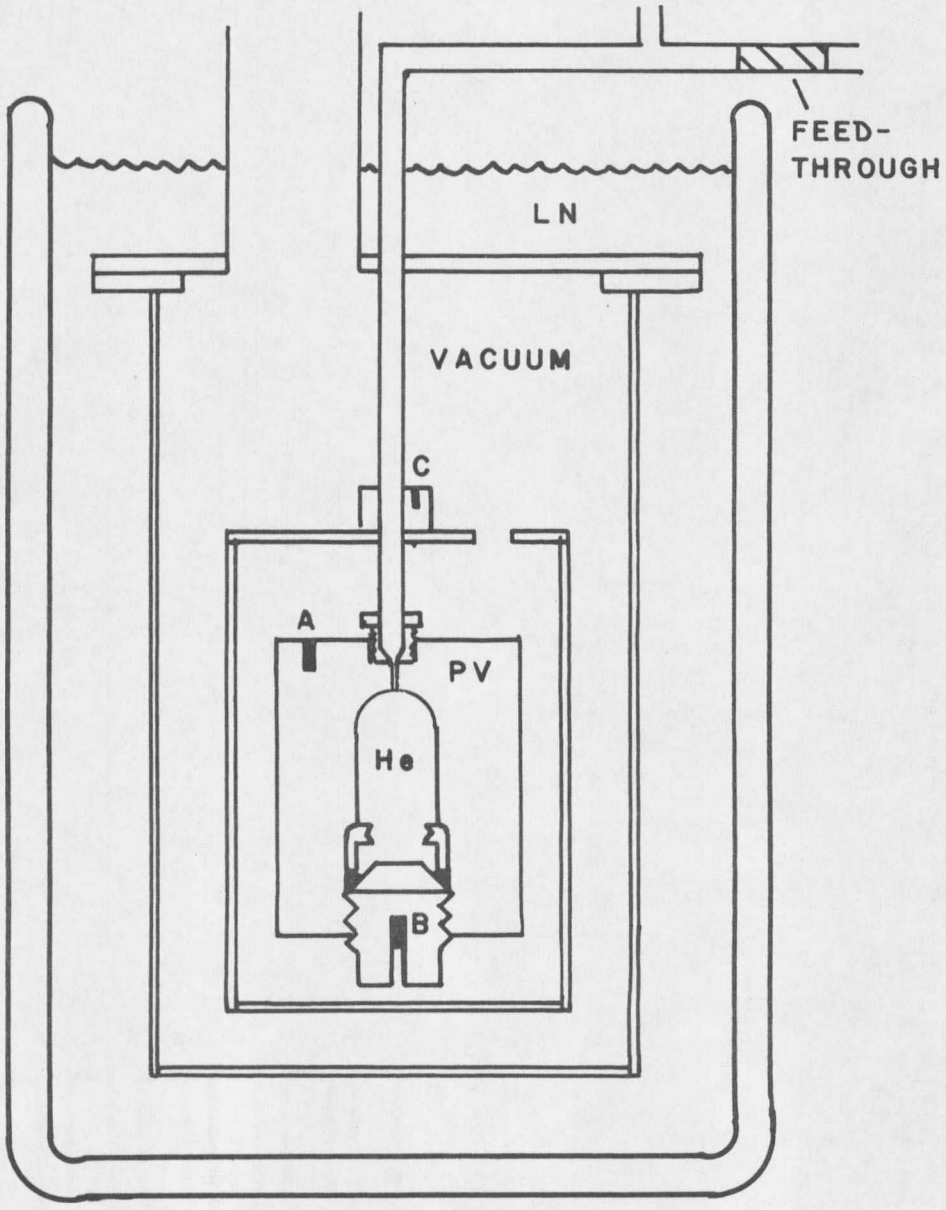

FIG. 10. Schematic drawing of cryostat assembly. Dark rectangular areas show location of temperature sensors.

tubing with soft solder and the body of the can slipped over the PV from below and attached to the can top with six screws. The top of the can has three $\frac{1}{2}$ in. holes allowing the space between the can and the PV to be evacuated and the electrical leads to reach the outside of the PV.

Surrounding this inner can is a 5 in. diameter brass can whose top is soft soldered to the pressure tubing. The large can is attached to its top by a vacuum flange. The top half of the flange is flat save a small ridge 1 mm wide and $\frac{1}{2}$ mm high. The lower half flange is completely flat. An aluminum foil gasket is pinched between the two pieces with pressure from a bolt ring. The extruded aluminum foil has acted as a vacuum tight gasket under liquid nitrogen for months without trouble. Off center on the top of the outer can is silver soldered a 1.5 in. diameter stainless steel tube through which the assembly is evacuated and leads for temperature sensors and heaters leave the cryostat. The entire assembly is supported by this tube which terminates in a tee. One side of this tee leads to the vacuum pump, and the other to a plexiglas flange through which shielded electrical leads are brought to ambient pressure. Finally the large brass can is immersed in a glass dewar of liquid nitrogen (LN), the top of the can being kept at least 4 in. below the LN surface.

The actual temperature regulation occurs in two steps. First the inner can is "roughly" regulated to ± 0.1 K by means of a heater

wound around a 0.75 in. copper rod concentric with the high-pressure tubing and attached to the lid of the inner can with silver solder. The heater current is regulated by the voltage of a grounded copper-constantan thermocouple attached to the copper rod. This point is operated about one degree below the PV temperature. This gives a point of approximately constant temperature along the pressure tubing and minimizes temperature gradients on the PV itself by minimizing heat transfer with its surroundings. The temperature gradient between the top and bottom of the inner can was measured with a differential thermocouple and found to be less than 0.1 K.

The second stage of regulation occurs at the top of the PV itself. A heater is wound around the outside of the PV and a temperature-sensitive capacitor controls the heater current. The capacitance sensor has a resolution of ± 2 mK and the top of the PV is stable to within this resolution. The temperature of the sample is assumed to be that of a second capacitance sensor located at the bottom of the PV in a hole drilled into the center of the closure plug. Extensive time histories were taken comparing the PV temperature with the sample properties. At the fastest scan rates used (~ 25 mK/hr) no more than a 5 min lag could be detected between heating and cooling. The difference between the top and the bottom sensor capacitance was sensitive to the amount of heater current supplied to the PV. When taking data, care was taken that this

difference was nearly constant, in order to maintain a constant temperature difference between the sample and the lower sensor. In immediate juxtaposition to the capacitance sensor in the closure plug hole was a copper-constantan thermocouple used to calibrate the capacitance sensor.

All heater wires and sensor leads were separately shielded. They were also thermally anchored to the cryostat at each stage of the temperature regulation by wrapping them several times around the appropriate can and the pressure tubing. No heat-conducting medium was smeared over them, however, as the heat transfer via the small diameter wires was calculated to be small compared to heat flow along the pressure tubing which acted as the main heat path from the PV.

4. Electronics for Temperature Control

The current to the shield can heater was controlled by the voltage of a copper-constantan thermocouple anchored close to the heater coil. The thermocouple voltage was compared to the voltage on a potentiometric voltage divider. The difference voltage was then measured by a Leeds and Northrup Model 9834 dc null detector. The recorder output of the null detector was in turn fed to the input of a voltage-controlled power supply which supplied the actual heater current. The voltage-controlled power supply was built

in this laboratory after a design by Kepco. Schematics of this arrangement appear in Figs. 11 and 12 which are taken from the Ph.D. thesis of R. S. Parker.[54]

The fine temperature control and measurement of the PV temperature employs a Model CSC 400 capacitance temperature controller marketed by Lake Shore Cryotronics.[52] This controller employs capacitance sensors made up of glass encapsulated strontium titanate.[55,56] The sensor capacitance varies with the temperature dependent strontium titanate dielectric constant. The useful range of this controller with the present reference capacitor is from 200 K to 1 K with the exception of a region around 65 K where the strontium titanate itself undergoes a phase transition and the slope of the heater current vs. temperature curve must be reversed. (A switch for this purpose is provided on the rear of the chassis.) An advantage of this controller is that the temperature calibration is not affected by magnetic fields, making it suitable for use in nuclear magnetic resonance experiments. In the temperature range near the KDP transition this instrument has a resolution of ± 2 mK.

The capacitance sensors were calibrated in situ against copper-constantan thermocouples using a Leeds and Northrup K-5 potentiometer and a distilled water ice bath reference.

An automatic filler was employed to maintain the liquid nitrogen (LN) level in the glass dewar in which the cryostat was

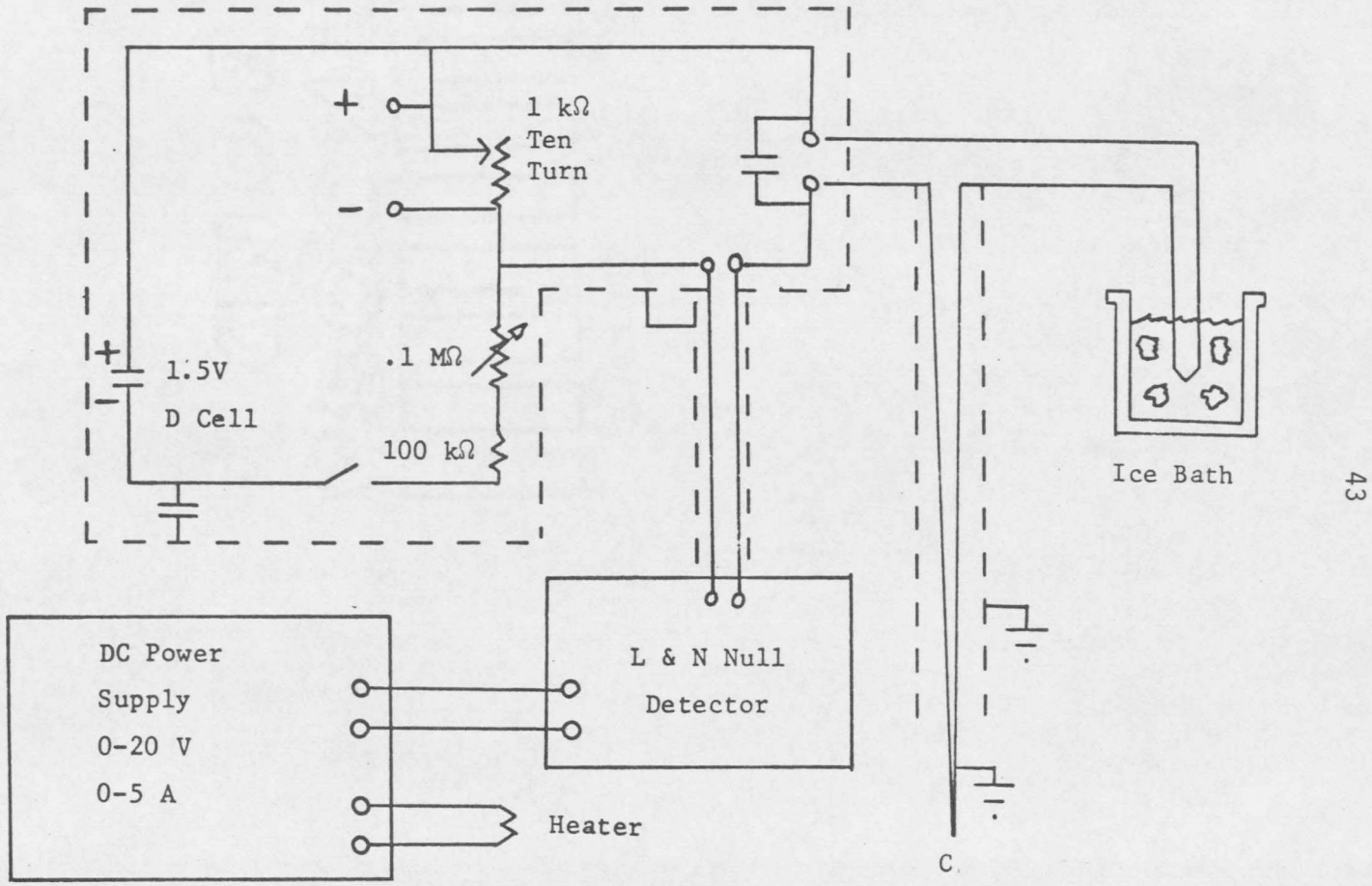

FIG. 11. Schematic of coarse temperature control system for shield can, after Parker.[54]

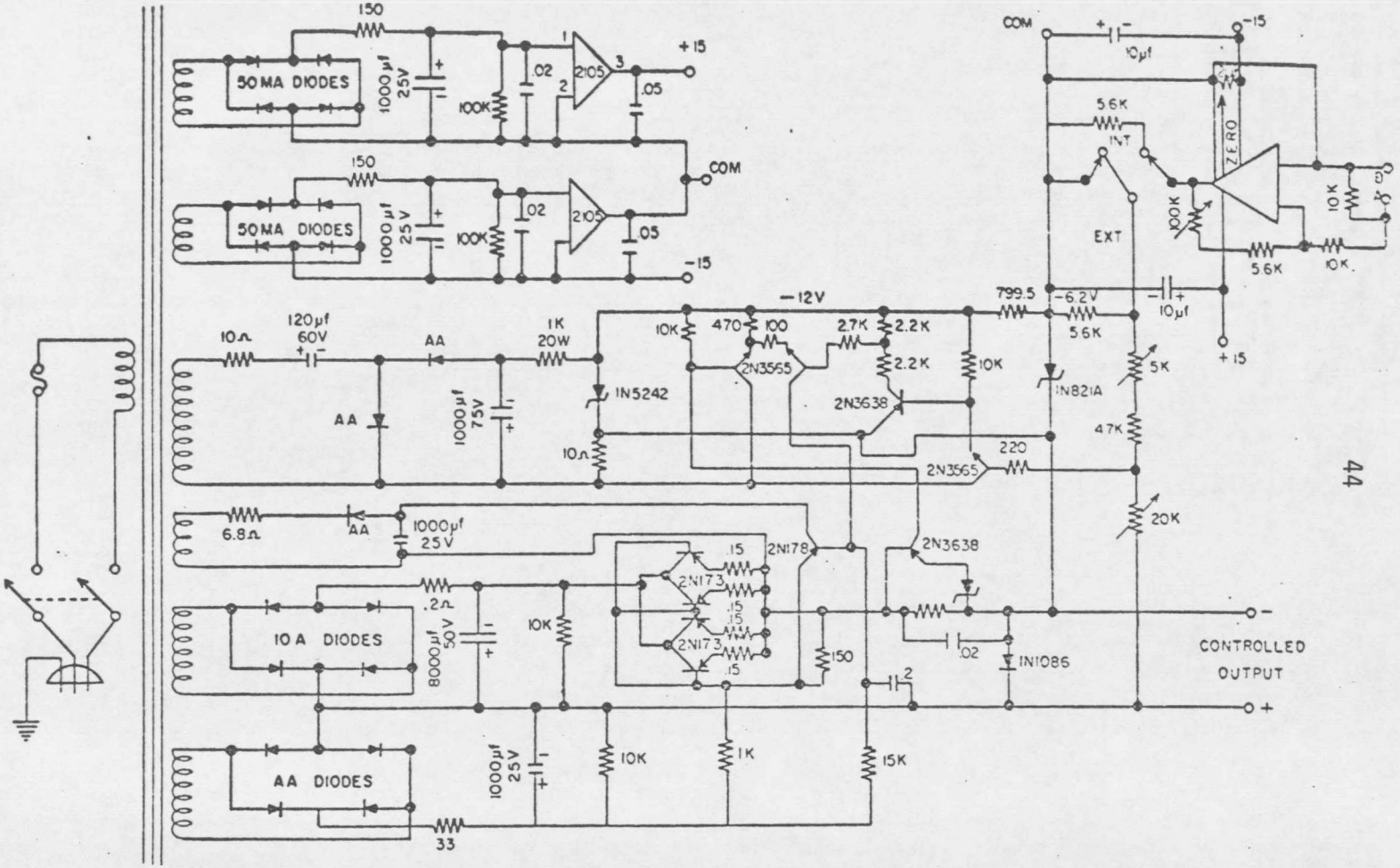

FIG. 12. Voltage controlled power supply, after Parker.[54]

immersed. The controller was assembled in the Physics Department electronics shop after a design by V. H. Schmidt. It employs a latching relay configuration controlled by two zener diodes used as level sensors. The zener voltage changes by a few tenths of a volt depending upon whether the diode is above or below the LN surface; this change is amplified by two cascaded transistors which control the relay supplying power to the solenoids controlling the air pressure above a reservoir dewar. Schematics of the filling system and the diode filler control are shown in Figs. 13 and 14.

5. Electrical Measurement of Crystal Properties

Dielectric properties of the crystal were measured in one of two configurations: a small signal ac bridge and a dc Sawyer-Tower[57] configuration.

ac Bridge

The small signal ac dielectric constant was measured using an ac Wheatstone bridge which employed a ratio transformer as two arms of the bridge. A Princeton Applied Research Model HR-8 lock-in amplifier was used as a phase sensitive null detector. No phase-compensating resistor was used in the bridge circuit as no phase difference was measurable between signal points A and B (see Fig. 13), and the small voltage perpendicular to the reactance remained constant throughout the transition region. No phase shift was

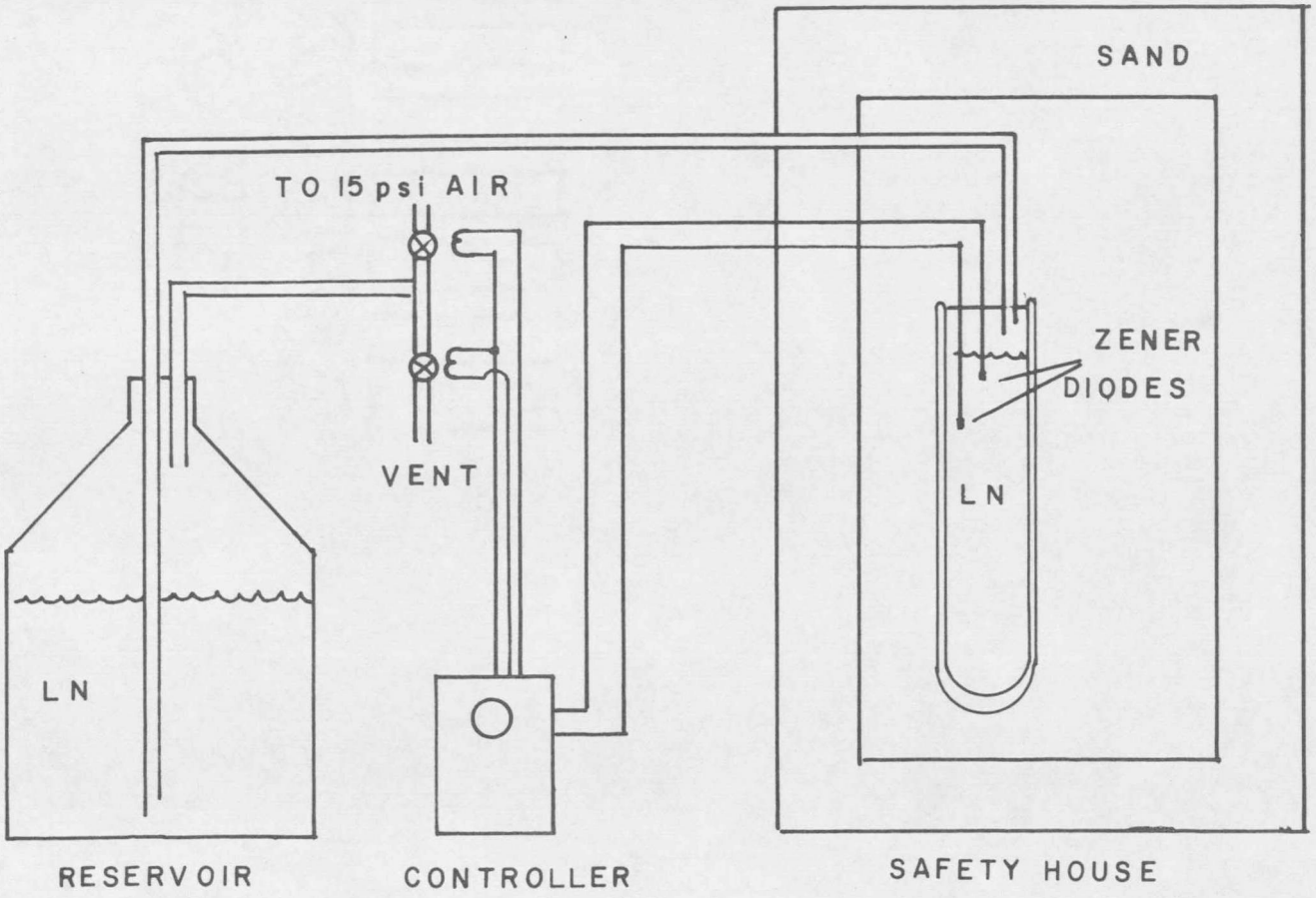

FIG. 13. Liquid nitrogen filling system.

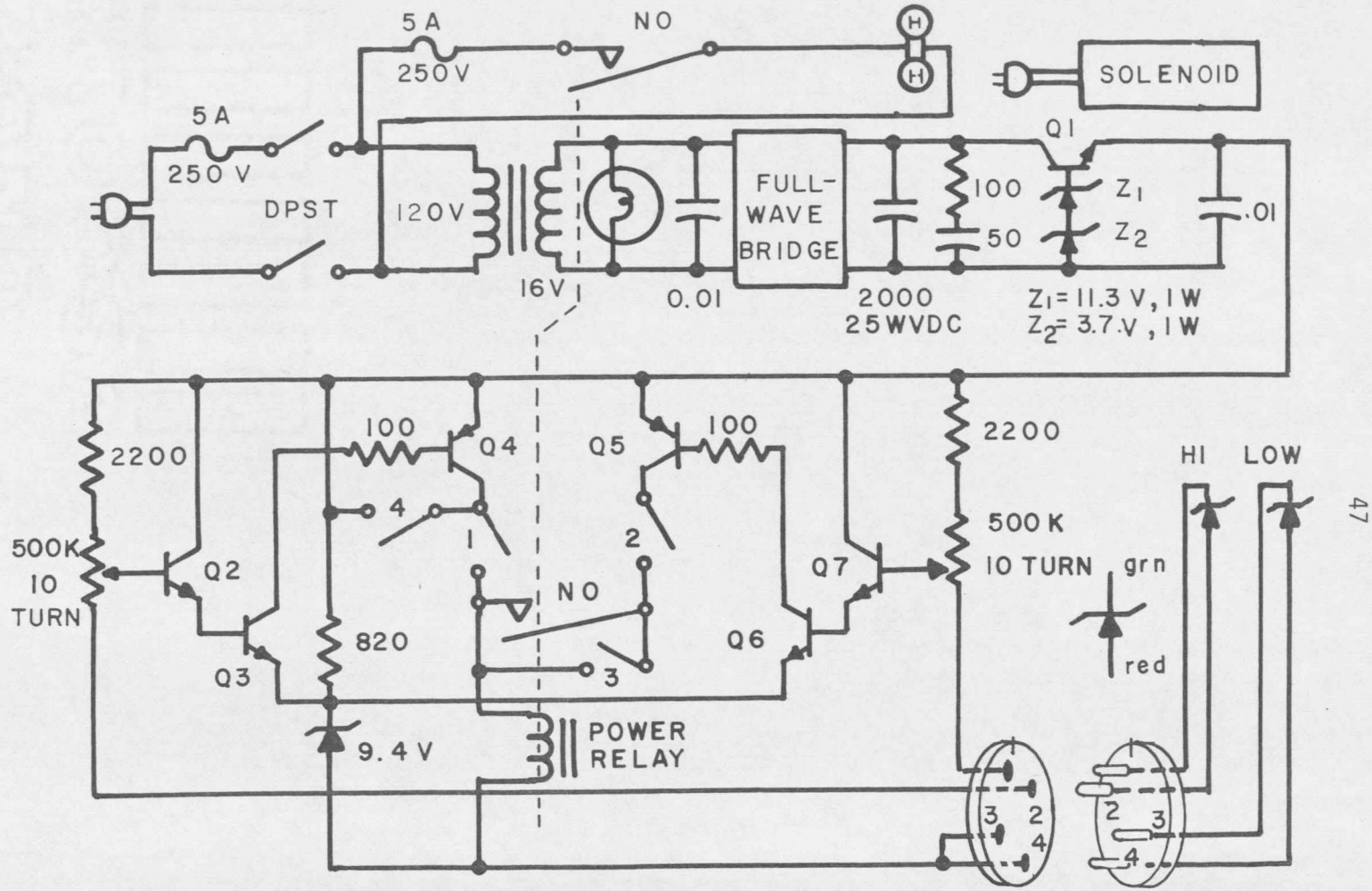

FIG. 14. Liquid nitrogen level control.

expected because of the low conductivity of KDP and the polystyrene reference capacitor, and the high Q of the ratio tranformer. As can be seen from Fig. 15, the value and position of the reference capacitor were chosen so that the input impedance of the HR-8 preamp and stray capacitance to ground had a negligible effect upon the measured values.

dc Measurements

The configuration used for quasi-static hysteresis loop tracing, isopol, and time constant measurements is shown in Fig. 16. An electric field is supplied to the sample using a battery and voltage divider. The polarization charge is stored on an 8 μf polystyrene capacitor. The voltage thus produced is measured by a Cary 401 vibrating reed electrometer with an input impedance of 10^{12} ohm. The recorder output of the electrometer was monitored with a Fluke Model 881A differential voltmeter or a Moseley Model 7000AR x-y recorder. The recorder output of the electrometer is also fed to a voltage follower and divider circuit which supplies a guard voltage equal to the input voltage seen by the electrometer. Leads to the electrometer input are guarded; sample No. 1 also included a guard ring configuration. In addition, all surfaces which might provide a charge path between the electrometer input and the guard or between guard and ground were scrupulously cleaned with acetone.

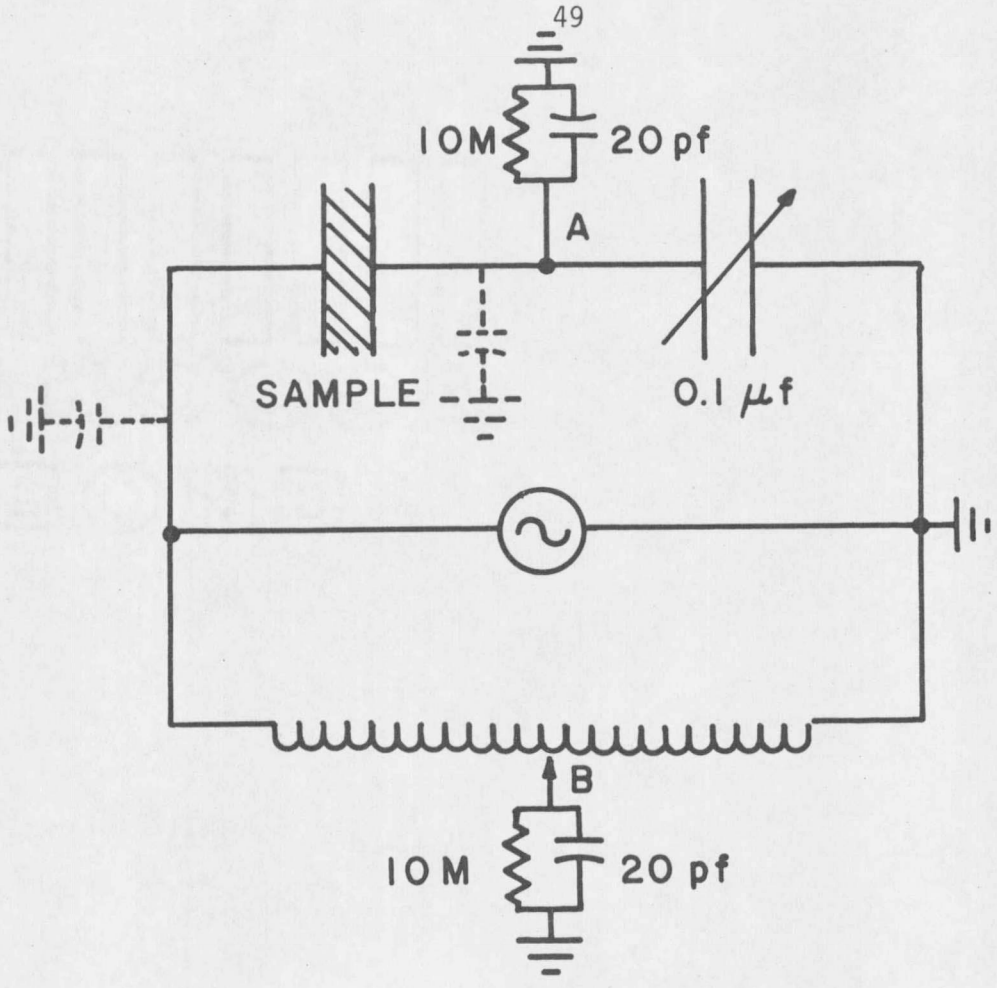

RATIO TRANSFORMER

HR-8 REFERENCE OUT

POLYSTYRENE CAPACITOR BOX

A&B HR-8 TYPE A PREAMP, A-B MODE

FIG. 15. Bridge circuit for ac dielectric constant measurements.

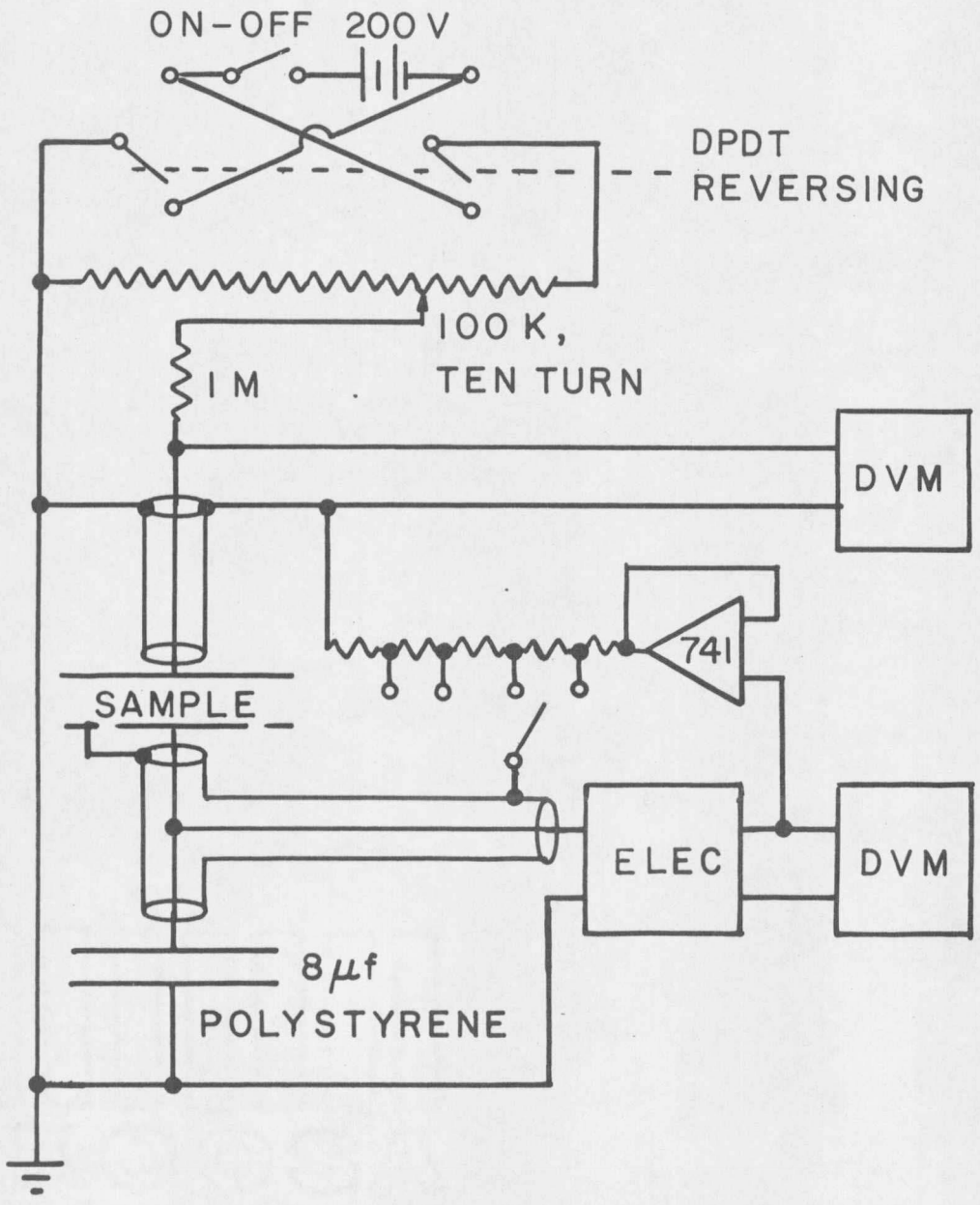

FIG. 16. Schematic drawing of dc polarization measurement circuit.

This included disassembly of BNC connectors and removal of all remnants of solder flux and fingerprints. Only Teflon insulation was used in this portion of the circuit with the exception of short (~ 4 in.) sections of wire at the high-pressure-to-air feedthroughs. Several epoxy-filled feedthroughs were constructed (details are given in the Appendix) and only one had sufficiently high insulation resistance (10^{12} ohm) to be suitable for use. Getting such high resistance appears to be a matter of good luck, as fabrication techniques did not change from one feedthrough to the next. The above precautions were sufficient to maintain leakage currents to a minimum and on the same order as the "leakage" to the electrometer input. A block diagram of this arrangement and a schematic for the voltage follower appear in Fig. 16.

During hysteresis loop measurements the potentiometer supplying the bias field to the crystal was varied with a clock drive. A fraction of the actual bias voltage was fed to the x input of an x-y recorder while the recorder output of the electrometer was fed to the y axis inputs.

During isopol measurements the E field was changed manually keeping the electrometer output, as measured by a Fluke Model 881A differential voltmeter, constant.

During measurements of the polarization relaxation time the electrometer output was once again connected to the y axis of the

x-y recorder, while the x axis was driven linearly in time. A step change in the E field (~ 5 V/cm) was effected manually, and the resulting change in polarization measured as a function of time.

6. Pressure System

The overall layout of the pressure generating system is shown in Fig. 17. There are two high pressure (HP) outlets: one using a liquid pressure medium, the other gas. The liquid system, shown in the heavier lines in Fig. 17, was used to test the integrity of PV's before use in the gas system. The PV may be charged to 20 000 psi directly with the hand pump. Higher pressures are obtained by closing the direct line from the pump to the PV (V-8) and opening value V-4, then pumping on the large diameter piston of the pressure intensifier. The pressure at the small diameter end is roughly multiplied by the ratio of large piston area to small piston area. Two precautions should be mentioned here: (1) Since the area ratio of the liquid intensifier is 23:1 and the hand pump could produce 20 000 psi, the resulting pressure on the HP end could be as high as 400 000 psi. This exceeds the pressure rating of all components including the intensifier. (2) Many commonly used hydraulic media solidify at high pressure (50 000 psi for 10W motor oil). Damage to gauges, intensifiers, etc. occurs in such cases. One must be sure of the pressure medium being used and its limitations. It is strongly advised that

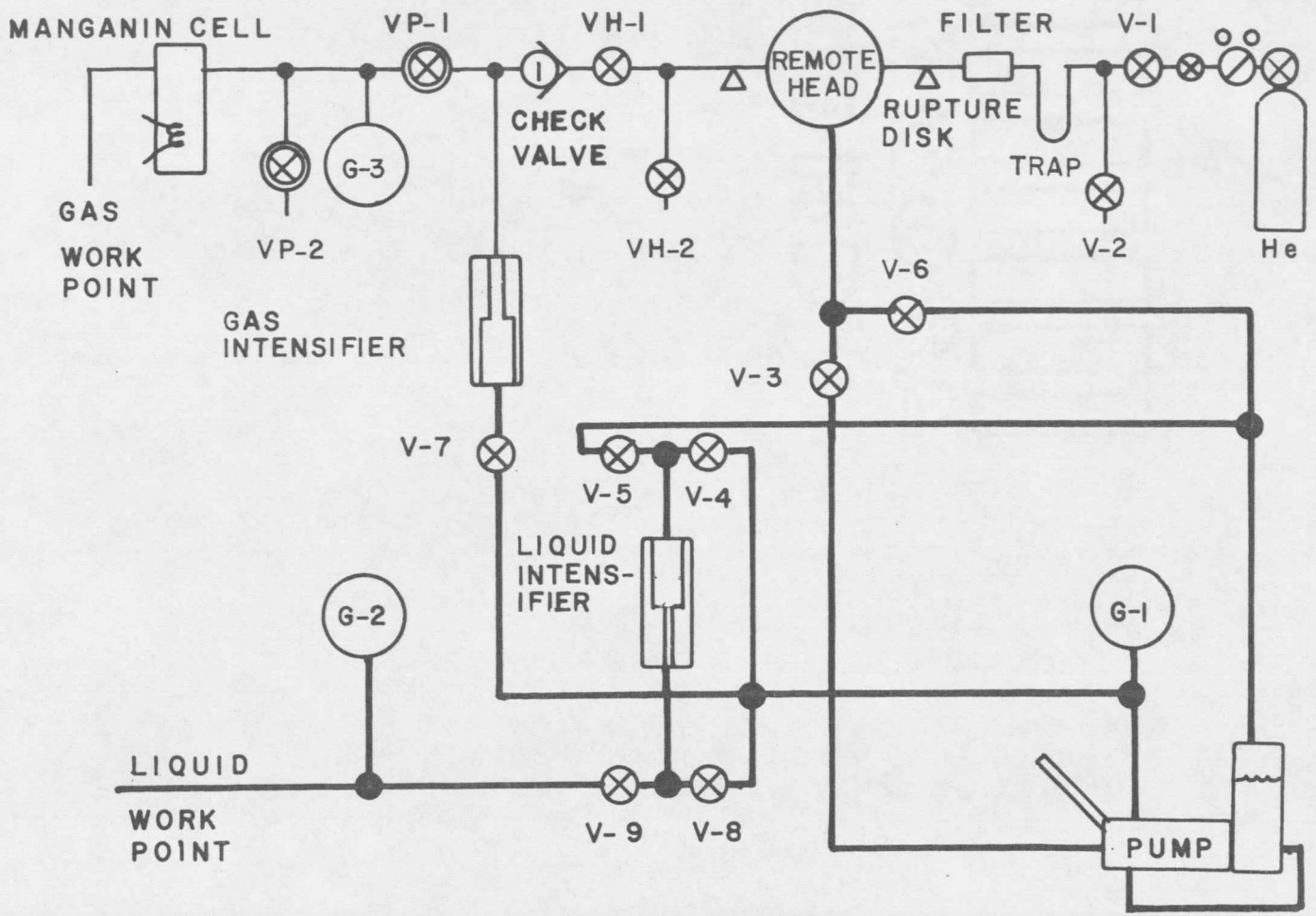

FIG. 17. Pressure generating system.

no attempt to use any part of the system be made without reading the Appendix which serves as an operating manual for this system.

In the gas system (lighter lines in Fig. 17) the gas flows from right to left starting at a bottle pressure of 3500 psi. This is immediately reduced by a standard regulator to 1450 psi. The gas is then passed through an LN-filled cold trap and a filter to the remote head. The remote head is a diaphragm pump much like the fuel pump in an automobile. Two check valves on the inlet and outlet respectively allow gas to pass only from right to left. Gas is drawn into and forced out of the head by means of a diaphragm driven by an oil line from the hand pump. The gas pressure downstream of the remote head may be raised to 14 000 psi by this means. Further increase in pressure is effected by means of the gas intensifier located downstream. Details, operating instructions, and precautions are found in the Appendix.

The pressure is monitored by measuring the resistance change of a coil of manganin wire which has a nominal pressure coefficient of resistance of $(\Delta R/R)/\Delta P=\alpha=1.67\times 10^{-7}$ bar^{-1}. These small resistance changes are measured by means of a Cary-Foster type[58] Wheatstone bridge arrangement, as shown in Fig. 18. In an actual Cary-Foster bridge the reference and sample resistors are interchanged during measurement, allowing the effect of contact EMF's to be subtracted out. In practice it was found that the necessary reversing switches

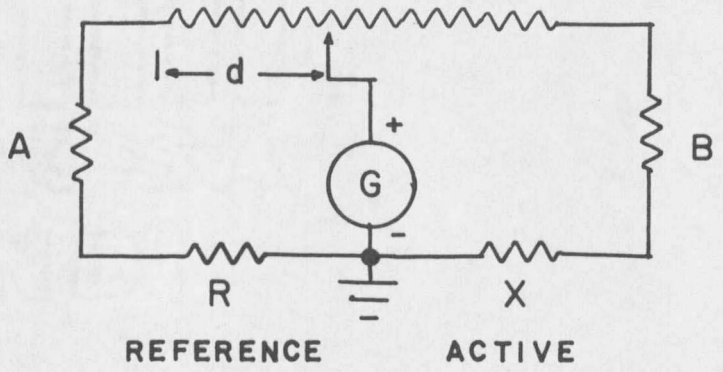

$R = 120.51\ \Omega$

$X_o = 120.36\ \Omega$

$\alpha = 1.651 \times 10^{-7}\ \Omega/\Omega/\text{psi}$

$r = 5.526\ \Omega$

$A = B = 100.00\ \Omega$

$\lambda = 5 \times 10^{-4}\ \Omega/\text{div}$

δ = No. of div. on slidewire

ξ = resistance change of active coil

P = pressure in psi

$$\delta = \lambda^{-1} R \left(\frac{A+B+r}{R+X_o}\right)\left(\frac{\xi}{1+\xi}\right)$$

$$\xi = \alpha X_o \text{"P"} = X_o(\alpha_o P - g P^2)$$

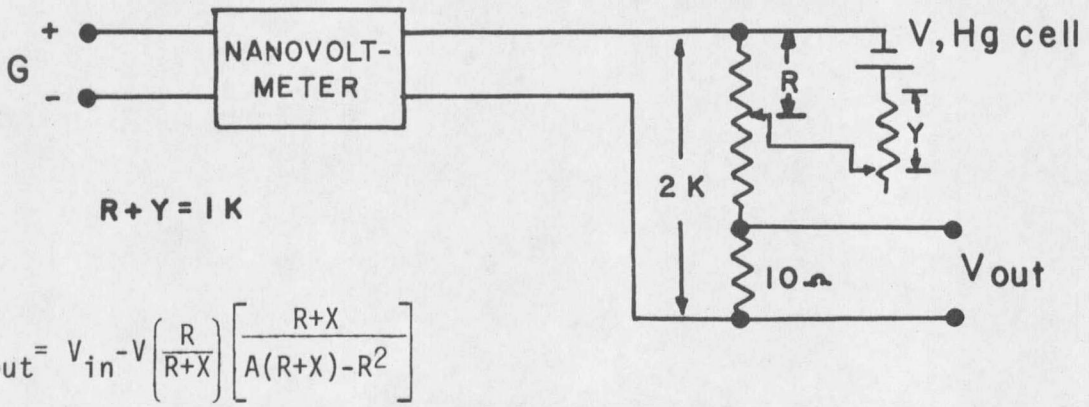

$$V_{out} = V_{in} - V\left(\frac{R}{R+X}\right)\left[\frac{R+X}{A(R+X)-R^2}\right]$$

FIG. 18. Cary-Foster bridge for pressure measurement.

introduced a great deal of noise into the null detector, and produced large uncertainties in contact resistance and thermal EMF's due to the use of dissimilar metals. Thus, it was decided to dispense with that facet of the bridge operation, preferring an increased ability to monitor small changes in pressure over a somewhat increased absolute accuracy.

The slide wire employed was from a Leeds and Northrup Type K potentiometer. This 5 ohm, ten-turn slide wire had 2×10^3 divisions and could be interpolated to give effectively 10^4 parts. Thus the effective resistance resolution was 10^{-3} ohm. (A change of one division added 5×10^{-4} ohm to one side and subtracted it from the other.) The manganin coil used[59] had an ambient pressure resistance of 120 ohm, hence the pressure resolution was $\Delta P = (\Delta R/R)/\alpha \doteq 50$ psi. On the other hand, the null detector used was a Keithley Model 148 nanovoltmeter. Operating on the 0.01 millivolt full-scale range the peak-to-peak noise was equivalent to approximately 1 psi. Thus the stability of the pressure, once set, could be monitored to a much higher precision than the actual pressure was known.

The bridge circuit was nominally compensated for ambient temperature changes by enclosing a matched reference coil of manganin wire in a cap atop the vessel containing the pressure sensing coil. Nonetheless, a substantial improvement in stability was obtained by enclosing the entire assembly in a styrofoam box filled with fiberglas

insulation, and thermostating the manganin cell housing. The temperature controller used was a commercial unit[60] with an estimated sensitivity of 0.05 K. The long term electrical stability of the entire pressure sensing unit was monitored at a known pressure of one atmosphere and found to be equivalent to ± 0.7 bar over a period of three days.

III. EXPERIMENTAL RESULTS

Section 1 is a discussion of the factors which led to the choice of static dielectric measurements as a means to determine the order of the KH_2PO_4 (KDP) phase transition. Section 2 is an introduction to the interpretation of constant polarization, isopol, data. In Sections 3 and 4 actual isopol data is presented for ambient and high pressure respectively. Section 5 contains a discussion of errors. Sections 6, 7, 8, and 9 are brief accounts of isothermal P vs. E, time constant, pressure hysteresis, and critical exponent measurements.

1. Dielectric Measurements of KH_2PO_4

The KDP ferroelectric phase transition appears unsuited for analysis by ac dielectric measurements. This is indeed unfortunate in that ac measurements near 1 kHz are relatively simple and may be carried out to high precision. Moreover, the distinction between first and second-order behavior of the dielectric constant in zero bias field is quite pronounced, as can be seen in Fig. 6. This difference is, however, obscured in the case of KDP by the fact that the dielectric constant in the ferroelectric phase immediately below the transition temperature, T_c, is quite high and essentially constant. The difficulty can be seen by comparing Fig. 9 with Fig. 6. The conventional wisdom is that this behavior is due to domain wall motion. Bornarel, Fouskova, Gagon, and Lajzerowicz[61] showed that the dielectric constant 12 K below T_c could be reduced from

4.5×10^4 to 1.4×10^4 by reducing the size of the applied ac field from 2 V/cm to 0.5 V/cm. This would seem to support the domain wall explanation. In the course of this investigation ac fields as small as 0.005 V/cm were used 0.05 K below T_c with no important reduction in dielectric constant. If domain wall motion is responsible for the high dielectric constant in the ferroelectric region, the walls are very mobile indeed immediately below T_c. In addition the dielectric constant could not be lowered by increasing the frequency to 10 kHz, above which the measurements become suspect owing to the distributed reactance of the great lengths of cable used to reach the crystal in the pressure vessel.

One might, nonetheless, hope to determine the order of the transition by ac measurements in the presence of bias fields and confined to the paraelectric region. This hope is thwarted by yet another of KDP's properties: a large electrocaloric effect. This effect manifests itself in the case of small signal ac measurements as an adiabatic correction.[18] The equation of state

$$E=A_0(T-T_0)P+BP^3+CP^5 \tag{14}$$

is obtained by differentiating H as in Eq. 13 with respect to P at constant T and X. One can then calculate the expressions for the adiabatic and isothermal dielectric constants,

$$(\varepsilon^T)^{-1}=(4\pi)^{-1}(A_0(T-T_0)+3BP^2+5CP^4) \tag{15}$$
$$(\varepsilon^S)^{-1}=(4\pi)^{-1}(A_0(T-T_0)+(3B+TA_0{}^2/C^P)P^2+5CP^4),$$

by taking the derivative of E with respect to P while holding the temperature and the entropy respectively constant. The difference stems from the difference in derivatives:

$$(\partial E/\partial P)_S=(\partial E/\partial P)_T+(\partial P/\partial T)_E. \qquad (16)$$

Jona and Shirane[18] show that the extra term on the right may be written as $(TA_o^2/C^P)P^2$. This adiabatic correction is larger than 3 $|B|$ thus making it impossible to determine the sign of B, and hence the order of the transition, in a straightforward adiabatic dielectric experiment.

Eberhard and Horn[45] have attempted to measure the order of the transition in an ac experiment using the thermal hysteresis of the transition. Such experiments rest on the assumption that the ratio of thermal hysteresis actually observed to that possible thermodynamically remains constant in increased bias fields. This is a point not in evidence and, indeed, unlikely, as the height of the free energy barrier separating stable and metastable states changes markedly with applied field and temperature.

Thus isothermal dielectric measurements within the paraelectric region appeared to the most promising for analyzing KDP. Okada[40] has determined the order of the KDP transition at ambient pressure by analyzing hysteresis loops taken at constant temperature and with very slow (200V/cm-hr) electric field sweeps. Similar measurements have been repeated in this laboratory and are reported in Section 5.

They are in general agreement with the constant polarization measurements described next. However, it has been found that even at such slow sweep speeds the results appear rate dependent. Attempts to repeat such measurements at high pressure were hampered by the need to periodically pump up the pressure to compensate for finite leak rates. Such pumping distorts the hysteresis loops. The dilemma is one of either reducing the value of the loops by tracing faster, or allowing the pressure to change by an amount great enough to alter T_0 by more than 2 mK, the experimental temperature resolution.

Owing to the above difficulties with previously used methods for determining the order of the KDP transition from dielectric measurements, it was decided to take equilibrium measurements of P, E, p, and T. The methods of analysis used are outlined in Section 2, and data is presented in Sections 3 and 4.

2. Isopols

There is a tradition in the literature of measuring polarization as a function of field (E) along isotherms, or as a function of temperature (T) along isochamps. Most of the data to be presented here is displayed as a function of T and E along lines of constant polarization, i.e. along isopols. This approach appears to be new and thus the following discussion is devoted to the interpretation of such plots. This discussion is based upon the Landau equation

of state (Eq. 14); however, many of the conclusions based on isopol plots are independent of this equation of state. The reader is cautioned not to equate the validity of all conclusions with the validity of the Landau expansion which is used here merely as a vehicle for introducing the isopol picture.

The equation of state which follows from the Landau free energy (Eq. 14), when rewritten, indicates that the isopols are straight lines in the T-E plane with slopes $(A_0P)^{-1}$ and E=0 intercepts $T_0-(BP^2+CP^4)/A_0$:

$$T=(A_0P^{-1})E+T_0-(BP^2+CP^4)/A_0. \qquad (17)$$

In the limit of small P the E=0 intercepts tend to T_0. If B is negative, as P increases the intercepts rise above T_0, and then fall as P increases further and the CP^5 term begins to dominate. For B positive the intercepts simply fall farther and farther below T_0 as P increases. The case for negative B is shown in Fig. 19. The initial increase and subsequent decrease in the T intercepts creates a region where isopols intersect. The first order line, FD in Fig. 19, lies within the overlap region which is bounded by caustics ACDB. BCE is the extension of a line similar to BD in the negative E half-plane not shown in Fig. 19. The critical point, D, is at a vertex of the curvilinear triangle formed by the caustics of intersecting isopols. Isopols are shown as solid lines when they correspond to an absolute minimum of the free energy. After crossing the first

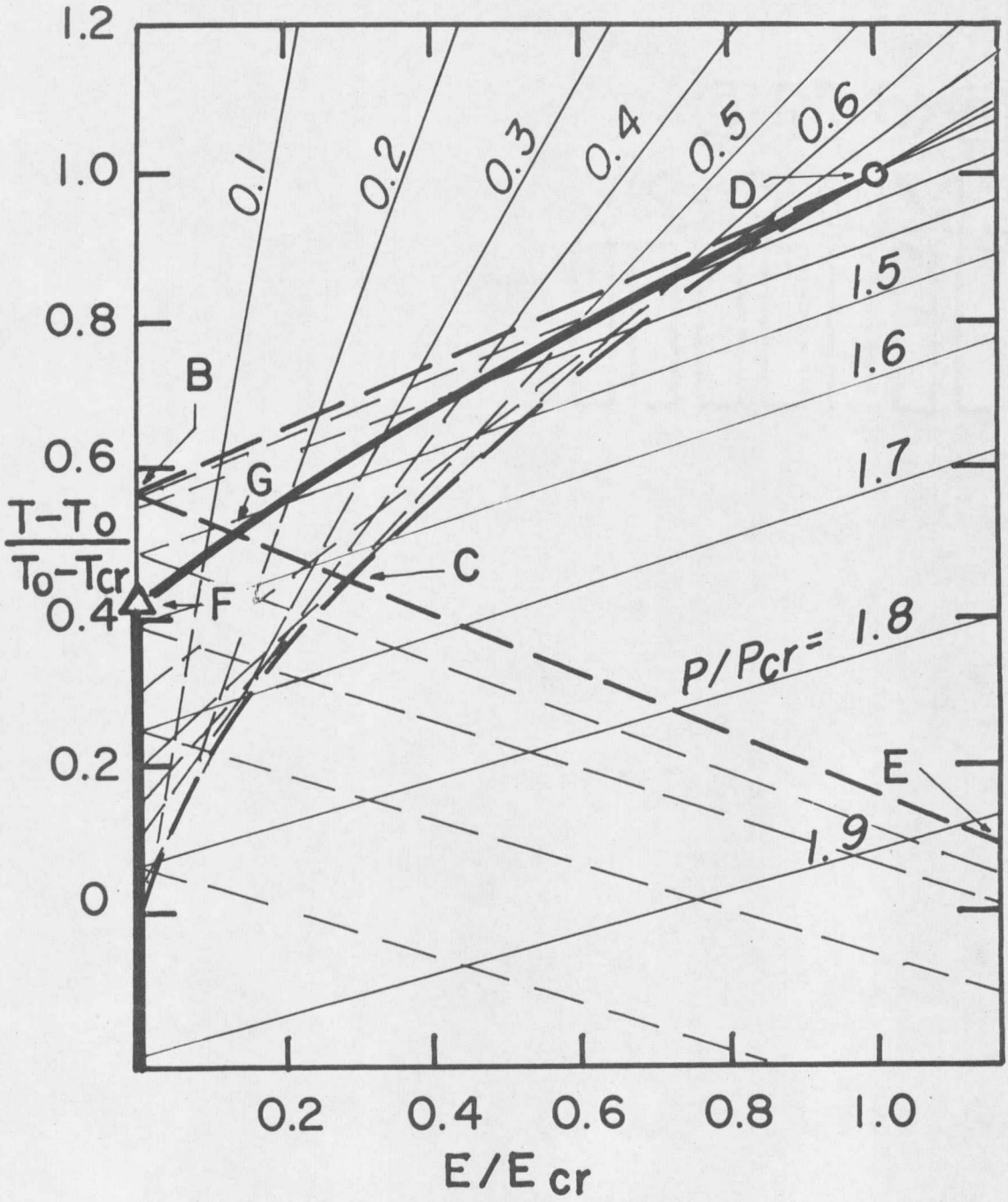

FIG. 19. Isopols as predicted from Landau equation of state: $E=A_o(T-T_o)P+BP^3+CP^5$.

order line they are shown as dashed lines and correspond to metastable thermodynamic states of the Landau free energy.

If metastable states are actually manifested by the crystal the regions of isopol overlap represent mixed phases. Denoting regions of polarization parallel to +E as "up", the mixed phase regions may be characterized as in Table III. It will be seen in data presented in Section 3, that when an isopol crosses a line such as CE in Fig. 19, it changes direction, heading almost vertically downward. This is interpreted as the formation of domains within the crystal. These are allowed by the Landau equation of state even though, on the basis of the free energy alone, such states are not energetically favorable.

In the Landau equation of state the order of the transition is indicated by the sign of the coefficient B, being negative for first-order and positive for second-order. In an isopol plot this difference manifests itself as a convergence or non-convergence of isopols, respectively. The deduction of the order of the transition from the behavior of isopols is, however, independent of the Landau equation of state. This may be seen by considering an isotherm drawn through an isopol plot just above T_{cr} (see Fig. 19). If the isopols are converging toward a $E \neq 0$ point, then the isotherm will encounter a large change in polarization for a small change in field near that point of convergence, i.e. the dielectric constant will be high. A dielectric constant higher at $E>0$ than at $E=0$ indicates

TABLE III. Possible mixed phase regions in Fig. 19. Phases corresponding to absolutely stable minima of the free energy are denoted S, states corresponding to relative minima are denoted M. The polarization is "up" when parallel to the applied E field.

Region	Para-electric	Ferro-electric "up"	Ferro-electric "down"
BDG	S	M	
CDG	M	S	
BGF	S	M	M
AFCG	M	S	M
ACE		S	M

a critical point, and thus a first order transition is implied. On the other hand, if the isopols do not converge except for E=0, a second-order transition is indicated.

The advantage of displaying data in isopol plots rather than as maxima in the dielectric constant is the numerical convenience and graphical clarity afforded by fitting straight lines. In addition, deviation from the simple Landau picture becomes obvious when the actual crystal isopols deviate from the high temperature extrapolations.

The method for extracting Landau parameters from isopol data is as follows. A least square straight line fit to paraelectric isopols is calculated. As follows from Eq. 14, A_o is obtained from the slopes of the isopols using

$$A_o=(\partial E/\partial T)_P/P. \qquad (18)$$

An approximate value of T_o is found from a plot of the extrapolated T(E=0) intercepts vs. P^2 for the three smallest isopols. This plot is a straight line and should extrapolate to T_o (see Eq. 17 and Fig. 26). The parameters B and C are then deduced from the intercept and slope respectively of a graph of $-A_o(T-T_o)/P^2$ vs. P^2. In practice T_o is then varied a small amount (within the experimental error) to produce the best straight line on this graph. In this latter procedure, points from the higher polarization isopols are heavily

weighted owing to the large scatter produced on this type of graph by the low polarization isopols for which $T-T_o$ is quite small.

3. Isopol Data at Ambient Pressure

Actual data for two different samples of KDP at ambient pressure are shown in Figs. 20 and 21. Convergence of isopols from the high temperature region toward a $E \neq 0$ point is obvious in both cases. This suggests that the transition is indeed first-order at ambient pressure. The solid lines drawn in Figs. 20 and 21 are the isopols as predicted by the Landau equation of state for the best fit parameters A_o,T_o, B, and C as given in Table II. As can be seen, the Landau expansion gives a good representation of the data throughout the paraelectric region. In the ferroelectric region major deviations occur when the isopols turn nearly vertically downward. This behavior is attributed to the formation of domains within the crystal. This belief is supported by the proximity of the "bends" to the mixed phase boundaries described in Section 2 of this Chapter.

The properties of the crystal as deduced from isopol analysis are in good agreement with properties measured by other techniques in a number of laboratories (see Table II). This gives increased confidence that deductions based upon isopol plots are valid, and strengthens arguments made at higher pressures where other data are as yet not available for comparison.

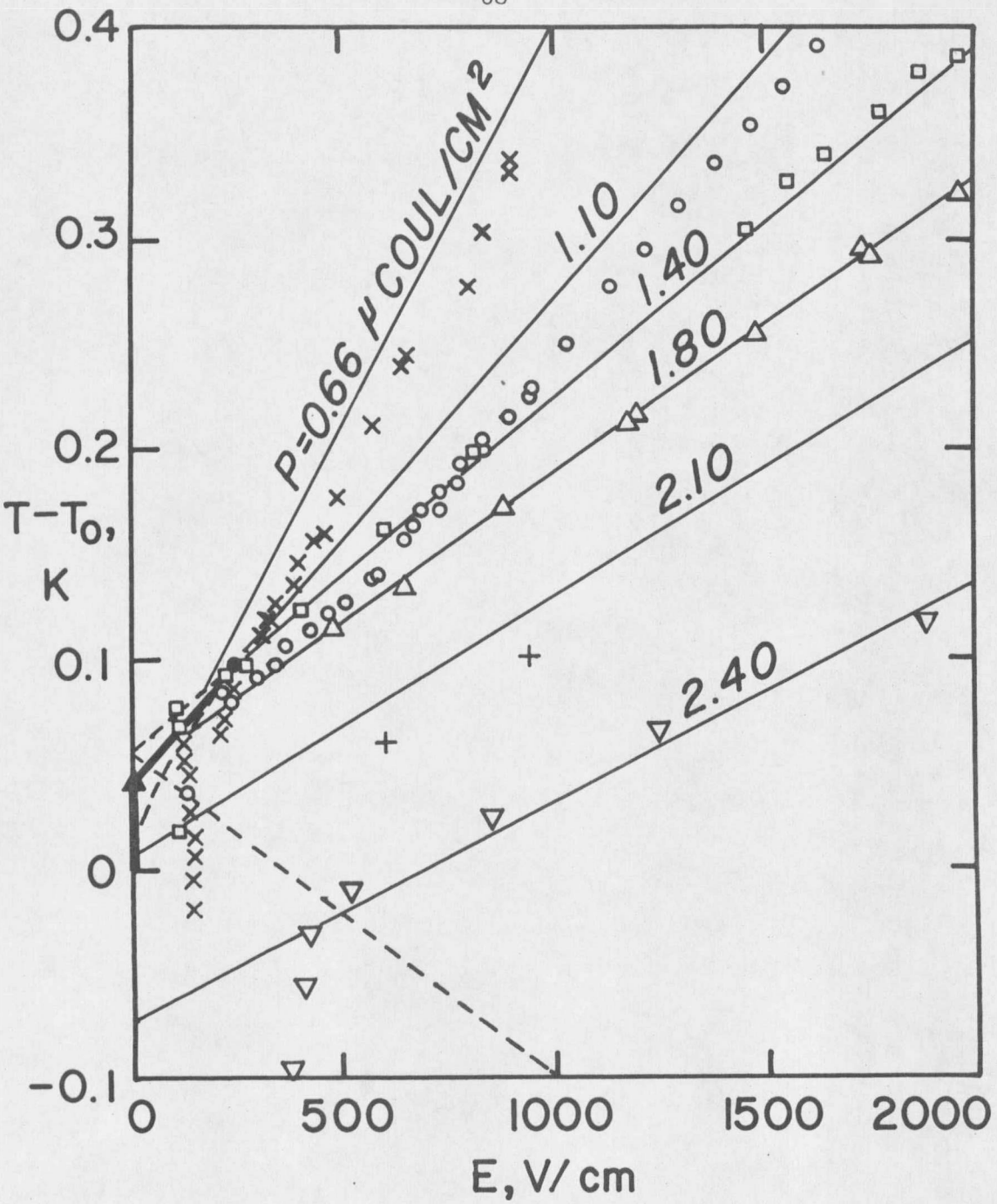

FIG. 20. Isopols of sample No. 1 at 0.001 kbar.

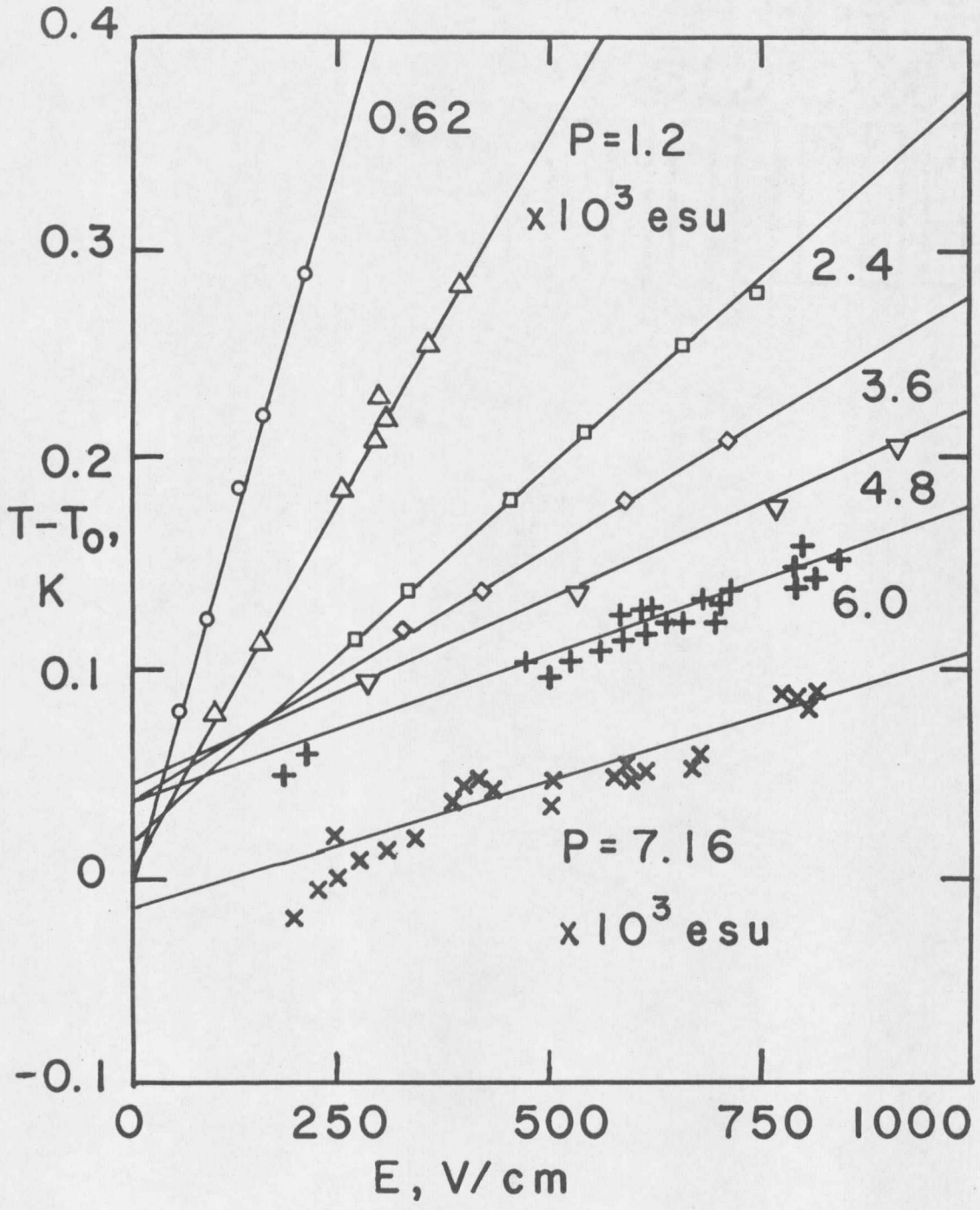

FIG. 21. Isopols of sample No. 2 at 0.0016 kbar.

4. Isopol Data at High Pressure

Data for sample No. 2 at pressures of 0.0016, 1.00, and 3.00 kbar are presented in Tables IV-VI and plotted in Figs. 21-23. The ambient pressure critical field of 186 ±60 V/cm is reduced to 43± 13 V/cm by 1 kbar of hydrostatic pressure based on the calculation of E_{cr} from the best fit Landau parameters. The Landau equation of state once again provides a good description of the data in the paraelectric region.

At three kbar the transition appears to be second order, that is, the extrapolated isopol intercepts all fall below T_o. The dielectric constant has its maximum value at E=0.

Fig. 24 shows a graph of $-A_o(T-T_o)/P^2$ vs. P^2 for sample No. 2 at three different pressures. The y-intercept of these graphs corresponds to B; the slope is C. Table VII summarizes the Landau parameters at the three pressures as deduced from the data using the procedure outlined at the end of Section 2 of this Chapter.

Table VII and Fig. 24 show that B values show a systematic, although apparently non-linear, increase with pressure. Comparison of the 1 and 3 kbar B values indicates B=0 at about 2 kbar, while a linear extrapolation of the decrease in B from 0 to 1 kbar indicates B=0 at about 2.5 kbar. The actual value probably lies somewhere in between.

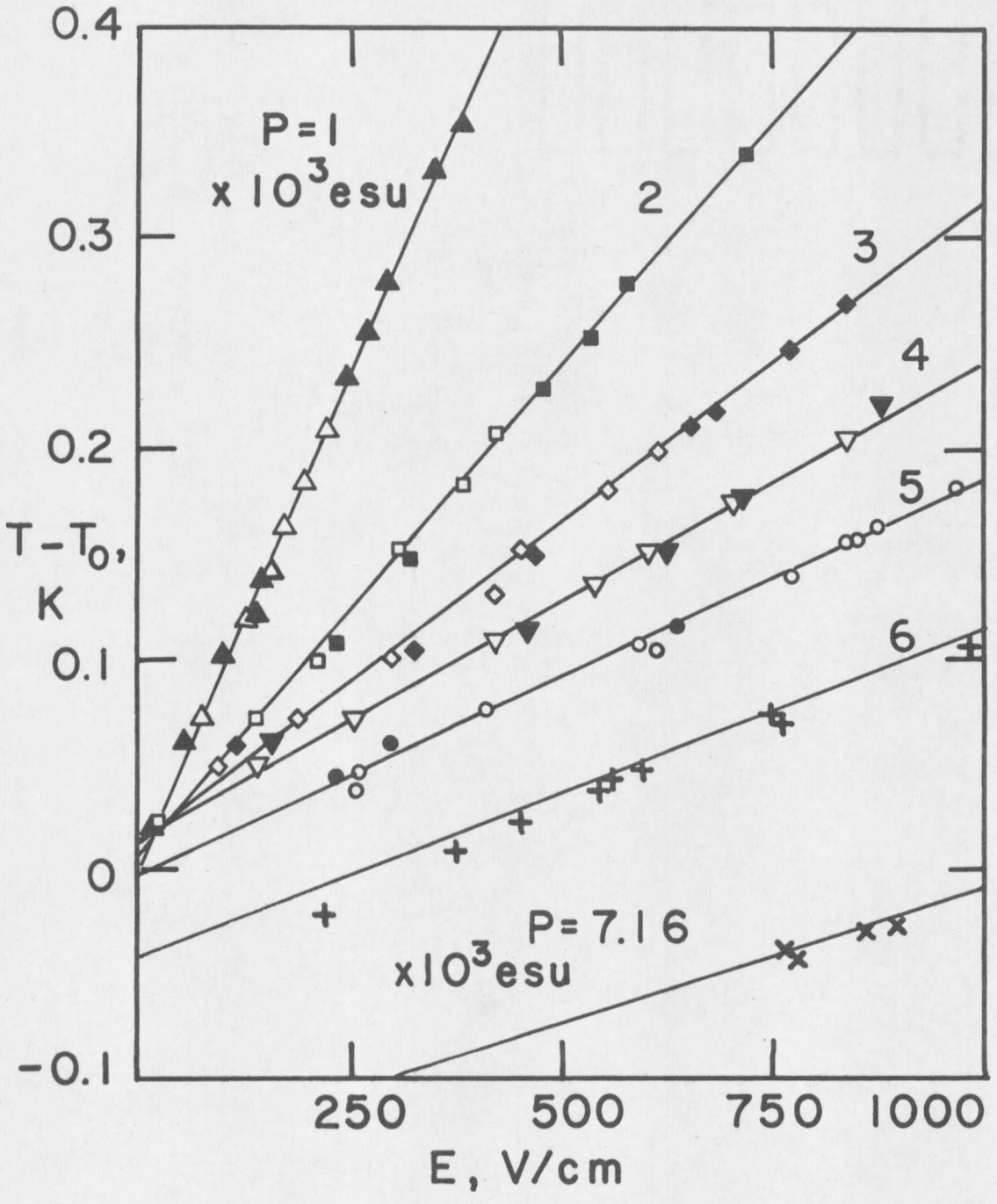

FIG. 22. Isopols of sample No. 2 at 1.00 kbar.

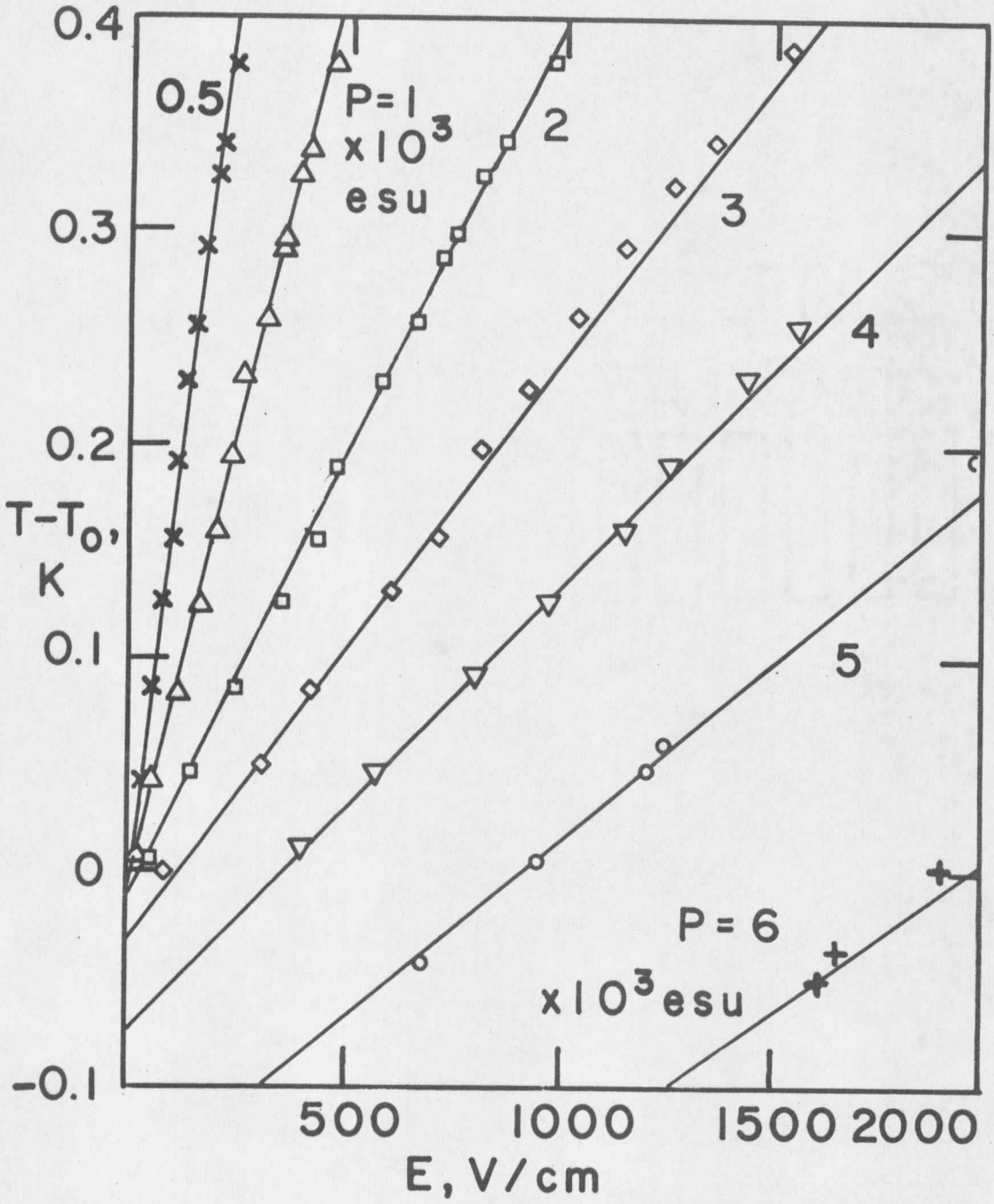

FIG. 23. Isopols of sample No. 2 at 3.00 kbar.

TABLE IV. Data for Sample No. 2 at 0.0016 kbar.

P, 10^3 esu	N	A_o, 10^{-3}esu	Standard Error 10^{-3}esu	95% Confidence Interval	$T-T_o$, mK	Standard Error, mK	95% Confidence Interval
0.621	7	3.91	0.05	0.13	9.8	3.0	7.7
1.194	8	3.90	0.047	0.12	4.9	2.8	6.9
2.388	6	4.07	0.06	0.17	27.2	2.8	7.8
3.582	5	4.21	0.029	0.09	47.3		
4.776	4	3.95	0.071	0.31	41.9	7.7	22.8
5.97	16	3.52	0.144	0.31	21.0	4.3	9.1
7.167	9	4.09	0.375	0.89	-12.5	6.7	15.8
		$\bar{A}_o$ = 4.01	$\sqrt{var}$=0.13	.19			

TABLE V. Data for Sample No. 2 at 1.00 kbar.

P, 10^3esu	N	A_o, 10^{-3}esu	Standard Error 10^{-3}esu	95% Confidence Interval	$T-T_o$, mK	Standard Error, mK	95% Confidence Interval
Decreasing Temperature							
1.00	12	3.62	0.062	0.14	2.7	4.2	9.4
2.00	10	3.61	0.081	0.19	7.6	5.5	12.7
3.00	6	3.81	0.15	0.42	21.4	6.7	18.6
4.00	4	3.80	0.14	0.60	23.2	4.5	19.4
Increasing Temperature							
1.00	8	3.62	0.084	0.21	3.1	3.6	8.8
2.00	6	3.56	0.114	0.32	7.6	4.5	12.5
3.00	6	3.74	0.12	0.33	20.5	4.5	12.5
4.00	6	3.60	0.05	0.14	15.6	2.0	5.6
5.00	9	3.52	0.064	0.15	- 2.7	2.2	5.2
6.00	8	3.56	0.165	0.16	-43.7	1.8	4.3
7.167	not calculated			assuming $\overline{A}_o$	-147.5	N A	N A
	$\overline{A}_o$ =	3.64	√var=0.11	0.08			

TABLE VI. Data for Sample No. 2 at 3.00 kbar.

P, 10^3esu	N	A_o, 10^{-3}esu	Standard Error 10^{-3}esu	95% Confidence Interval	$T-T_o$, mK	Standard Error, mK	95% Confidence Interval
0.50	14	4.23	0.085	0.19	+10.6	5.8	12.6
1.00	15	4.13	0.071	0.15	- 2.4	4.8	10.4
2.00	16	4.09	0.054	0.12	-15.8	3.8	8.1
3.00	16	4.10	0.054	0.12	-30.0	4.0	8.6
4.00	9	3.90	0.085	0.20	-82.4	5.2	12.3
5.00	5	3.74	0.039	0.12	-169	2.4	7.
6.00	3	3.53	0.106	1.35	-309	8.0	101.
	$\overline{A_o}$=	4.04	$\sqrt{var}$=0.18	0.20			

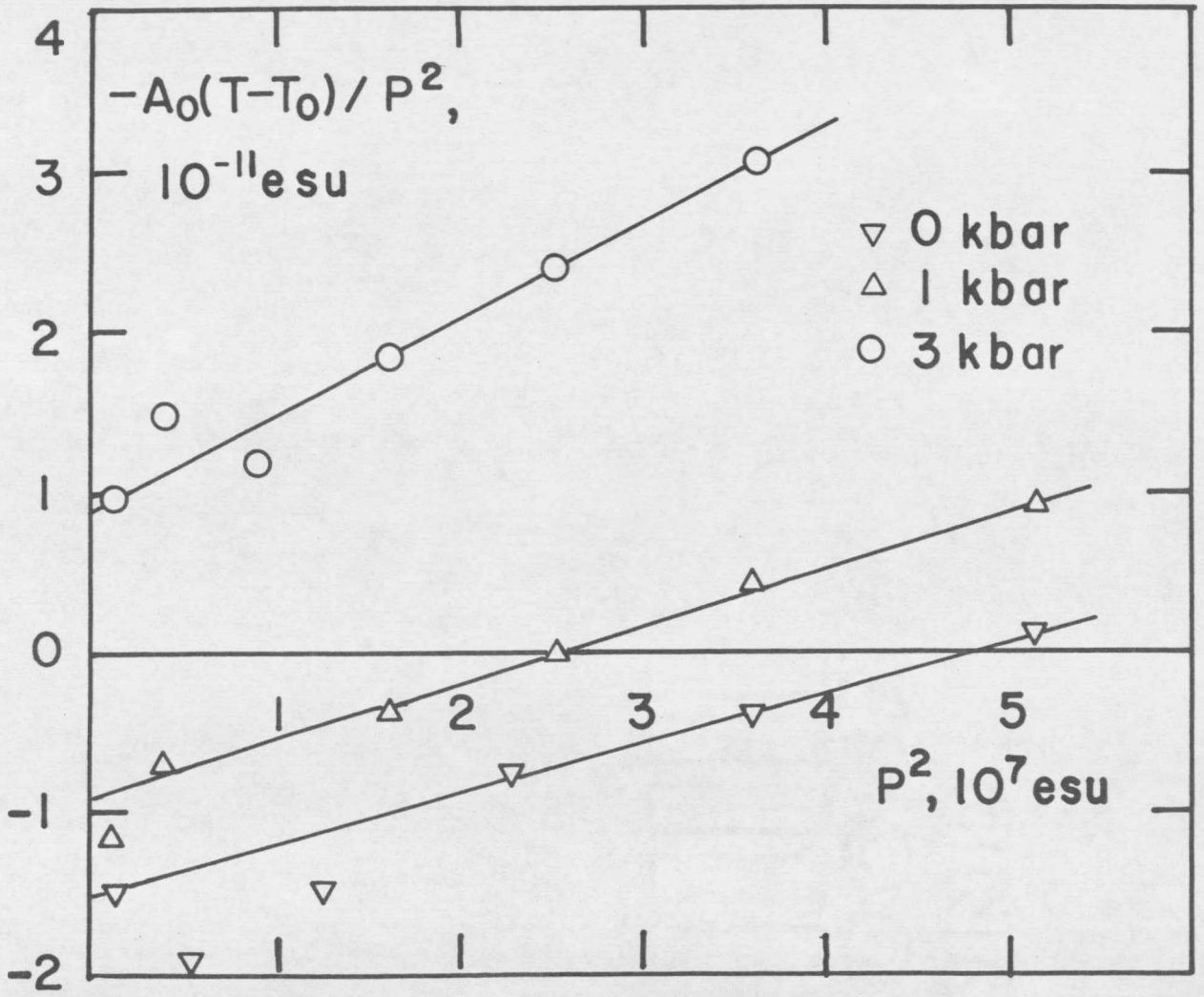

FIG. 24. $-A_0(T-T_0)/P^2$ vs. P^2 at 3 pressures.

TABLE VII. Landau parameters for Sample No. 2 as a function of pressure.

Pressure* kbar	T_o# K	$dT_o/d\rho$ K/kbar	A_o 10^{-3}esu	B 10^{-11}esu	C 10^{-19}esu	$T_{cr}-T_o$ K	E_{cr} V/cm
0.0016	122.12±0.1	-4.54±0.05 †	3.93±0.2	-1.48±0.1	3.1±0.4	0.081±0.03	186±60
1.00±0.002	117.72±0.1		3.64±0.1	-0.89±0.1	3.6±0.4	0.027±0.01	43±13
3.00±0.002	108.24±0.1		4.04±0.2	+0.90±0.1	6.1±0.4	NA	NA

*Stable to ±0.0005 kbar

#Absolute calibration not tied to National Bureau of Standards

†Not measured differentially due to scale change

NA Not applicable, transition is second-order

5. Errors

Standard errors and confidence intervals for the slopes and intercepts of isopols were calculated in the usual way. The Montana State University Math-Stat library program MREG[62] was used. Standard errors are in general agreement with the claimed temperature resolution of ±2 mK combined with pressure induced T_o variation of ±2 mK.

Error bars are deliberately omitted from Fig. 24 in favor of Fig. 25 which shows the effect of varying T_o by ±0.01 K about the best value. Similar results obtain if T_o is held fixed and the isopol intercepts varied. When $T-T_o$ is on the order of the standard error in T the scatter in such a plot is large indeed. This is not to suggest, however, that intercept data from the lowest polarization isopols is not significant in indicating the transition order. If, instead, one chooses to graph T(E=0) vs. P^2 for the lowest polarization isopols, as in Fig. 26, one finds a difference in the sign of the slopes between the first-order (0 and 1 kbar) and the second-order (3 kbar) data which is unequivocal even if 95% confidence intervals are used as error bars.

Because of the large uncertainty in the $T-T_o$ values for the low polarization isopols only the high polarization isopols were used in the least squares fits from which best values of the B and C parameters were deduced. Then T_o was varied slightly to bring the low polarization intercepts into agreement. The final justification

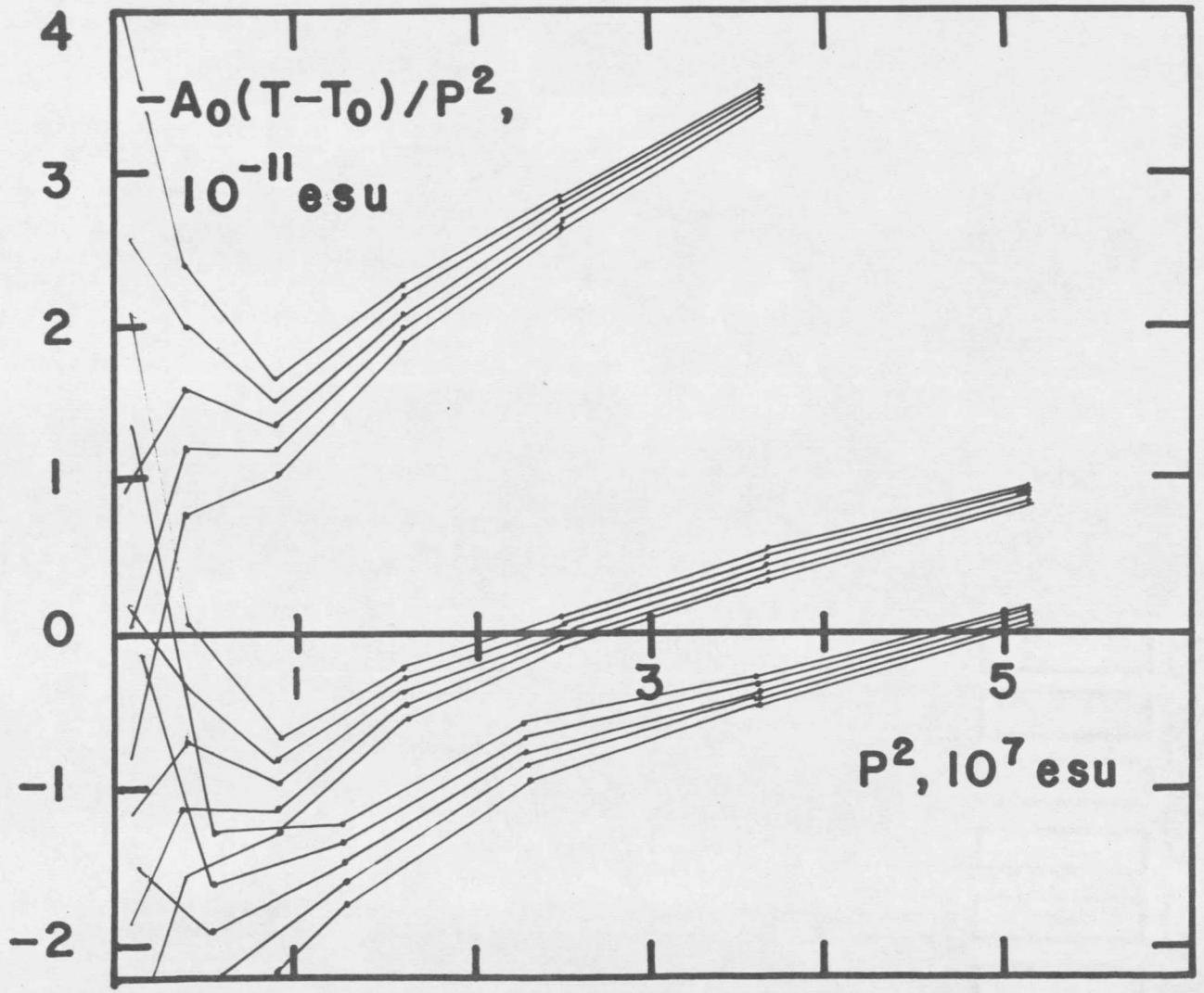

FIG. 25. Effect of the variation of T_0 by ± 0.01 k on Fig. 24.

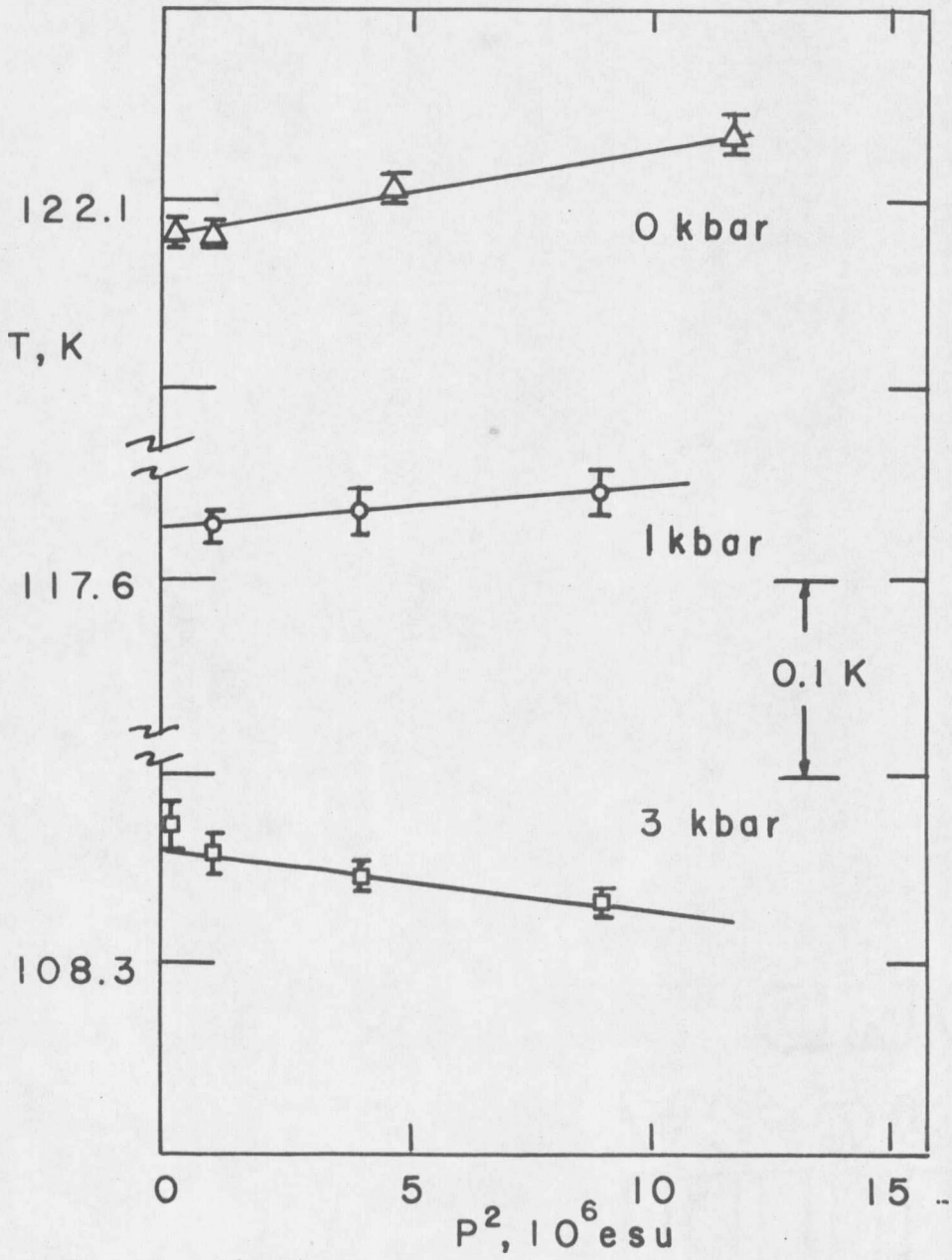

FIG. 26. T(E=0) intercepts of low polarization isopols, described by $T(E=0)=T_o+(B/A_o)P^2$. Relative displacements on vertical scale arbitrary. Slope change indicates change in the sign of B.

for this process is the good agreement with the original polarization data which this procedure produced.

6. Isothermal P vs E

In addition to the above isopol plots, isothermal measurements of the polarization as a function of slowly varying E field were made at 0.5 and 3 kbar. Double hysteresis loops similar to those reported for KDP at ambient pressure were produced at 0.5 kbar. These have been interpreted as indicating a first-order transition.[63] In addition, the P-E curve starting from P=0, E=0 is a graph of the equation of state. From this curve values of B and C may be deduced as Okada[40] did, following a method due originally to Sidnenko and Gladkii.[35] This technique was used and the resulting Landau parameters found to be in reasonable agreement with those deduced from isopol plots. However, these values appeared to be sweep rate dependent even at E field sweep rates as slow as 240 V/cm-hr. For this reason a great deal of confidence is not placed in the exact value of the parameters so deduced. Nonetheless, the general shape of these curves is highly significant. If on a P vs. E graph the actual curve rises above the extrapolation of the straight line portion of the curve near the origin, the dielectric constant is necessarily greater during that rise indicating a $E \neq 0$ critical point. If the curve falls only below the extrapolated straight line no such point

is indicated. Fig. 27 shows just this difference between the 0.5 and 3 kbar P-E traces.

7. Time Constants

Time constants of the polarization response were measured at ambient pressure. The hope was that these could be used to identify the critical point and then compared to similar measurements at high pressure. Measurements were made by perturbing an equilibrium T, E, P configuration by manually increasing the field in a small step ($\Delta E \sim 5$ V/cm) and observing the return to equilibrium as a function of time (t). The 1/e time constants were then deduced from a plot of log P *vs.* t. The values found are shown in Fig. 28. They are generally 4x longer than those found by Okada.[39] It is noted that lines of constant time constant are very nearly isopols in the paraelectric region. Measurements of time constants in the immediate neighborhood of the critical point were difficult to obtain owing to their increased length. On one occasion (marked ∞ in Fig. 28) the change in polarization produced by ΔE was larger than the initial polarization and showed no sign of halting its upward creep in over a half hour.

At elevated pressures time constant data was not taken owing to the lack of complete equilibrium caused by finite leak rates and perturbations caused by intermittent pumping.

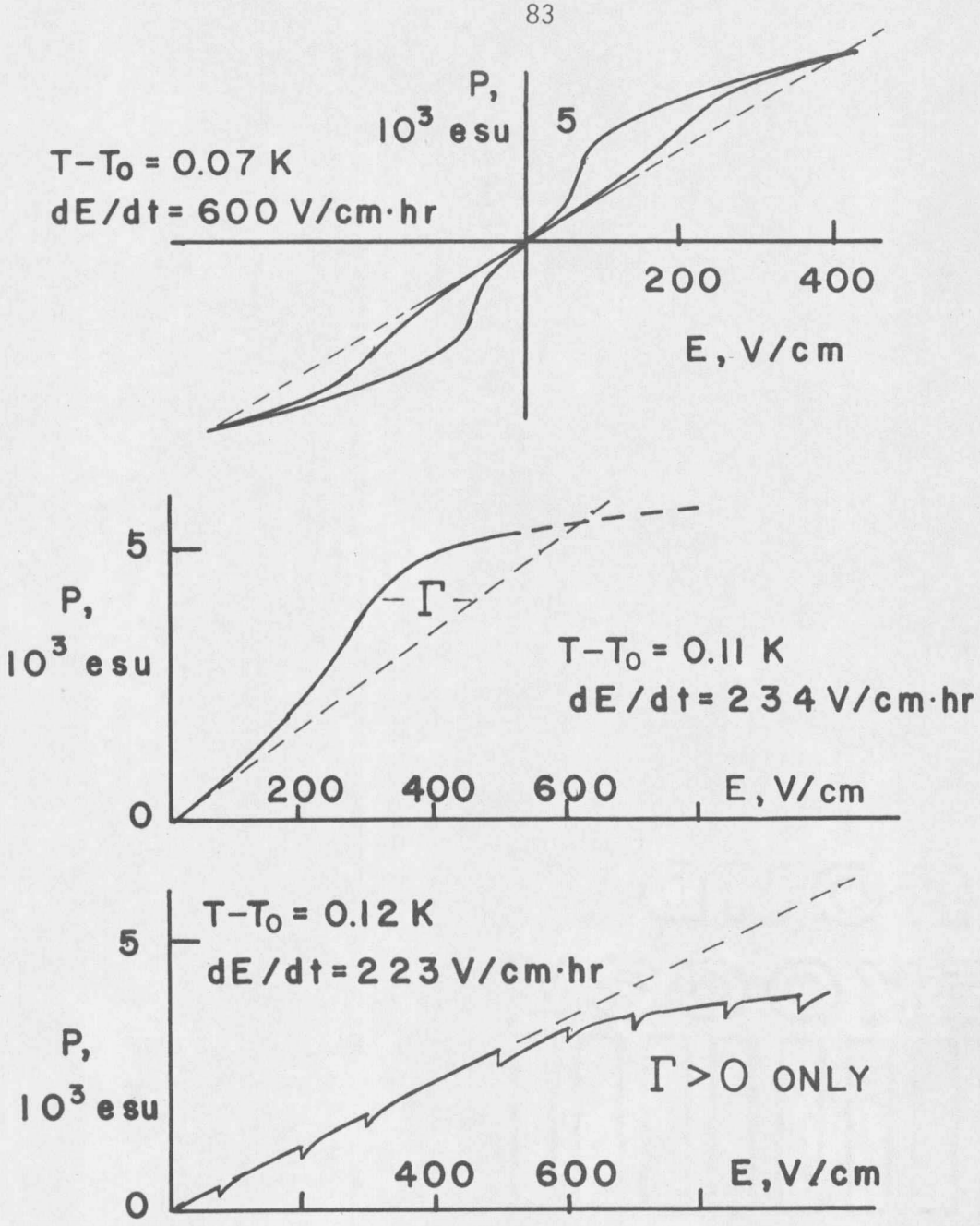

FIG. 27. Isothermal P vs. E plots at 0.5 and 3 kbar. Here $\Gamma = E - A_0(T-T_0)P = BP^3 + CP^5$. Spikes at 3 kbar are due to pressure pumps.

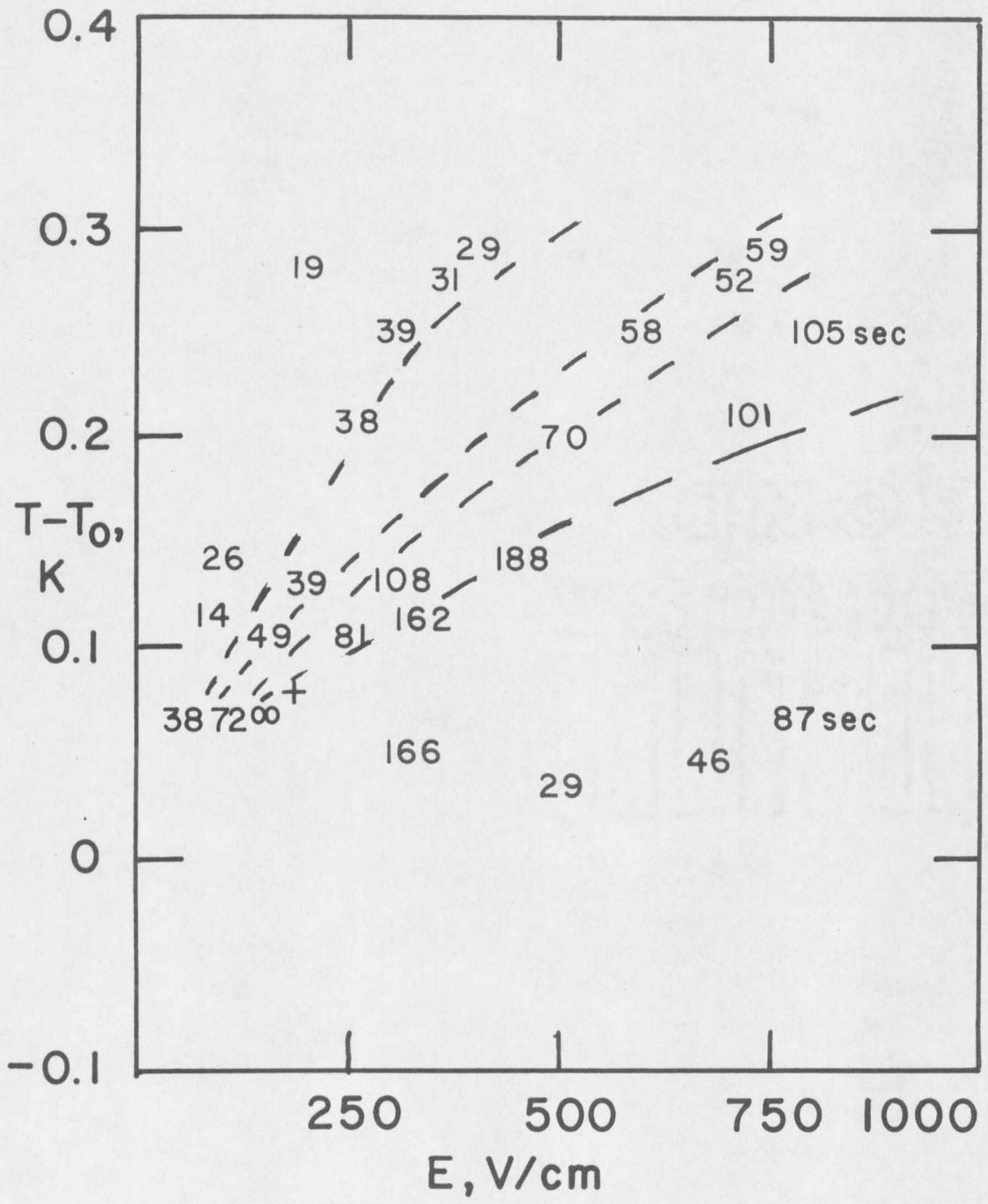

FIG. 28. Time constants for polarization relaxation at 0 kbar. The + marks the critical point as calculated from isopol data.

8. Pressure Hysteresis

In addition it should be noted that a pressure hysteresis in the value of T_o, and in some cases A_o, has been noticed. In order to maintain the pressure of the system constant to within ±0.25 bar, it was necessary to pump the system at intervals ranging from 30 min at 3 kbar to 2 hrs at 1 kbar. If a set of isopols was begun one day, and the system left overnight without pumping, upon returning to the standard pressure the crystal would almost invariably show a shift in T_o as deduced by a systematic shift in the isopols. Unless otherwise noted all of the data presented refers to single runs lasting around the clock, often for several days.

In the case of the 1 kbar data two sets of isopols taken a full week apart show identical (to within experimental error) isopol structure except for T_o even though one was taken as temperature was increased and the other as temperature decreased. On the other hand, the three kbar data showed a shift in both T_o and A_o when left unpumped only 8 hours. This type of hysteresis makes it difficult to determine the parameters of the crystal unambiguously as a function of pressure.

9. Critical Exponents

The only critical exponent directly accessible to measurements made here is γ, the exponent for the dielectric susceptibility:

$$\chi \sim ((T-T_c)/T_c)^{-\gamma} = \varepsilon^{-\gamma}. \qquad (19)$$

Since $\chi = dP/dE$ one may write for small ΔP and ΔE that $\Delta E = \Delta P \varepsilon^{-\gamma}$. Thus it can be seen that the mean field value of 1 for γ follows from straight line isopols. At 3 kbar the $P = 0.5 \times 10^3$ esu isopol indicates $\gamma = -d(\log E)/d(\log \varepsilon) = 1.03 \pm 0.04$ to within 0.02 K of T_c. The error interval is the 95% confidence interval. Indirectly, mean field values for other exponents in the paraelectric region are implied by the fact that the data can successfully be fit by the mean field Landau expansion.

Data in the ferroelectric region does not obey a simple equation of state, neither does it scale with mean field exponents. This behavior is attributed to the formation of domains within the crystal and one's subsequent inability to measure the true intradomain polarization, rather than any breakdown of mean field theory or scaling laws.

IV. DENOUEMENT

1. Summary

This investigation began with the conjecture by V. H. Schmidt[16] that a tricritical point might be produced in the phase diagram of KH_2PO_4 (KDP) by the application of hydrostatic pressure. If this were the case, KDP's paraelectric to ferroelectric transition would alter from first-order at ambient pressure to second-order at high pressure, the point of cross-over being the tricritical point (TCP). If there were a TCP the two critical points at the terminations of the first-order line in the temperature (T) and electric field (E) plane would merge at E=0. At the time of this conjecture, however, there was some doubt (in the mind of at least one reviewer) that the transition was in fact first-order at ambient pressure. Even amongst those experiments which supported a first-order transition at ambient pressure, there was disagreement as to the coordinates of the critical points.

Hence the purpose of the experiments described in this thesis was to (1) resolve the controversy regarding the coordinates of the critical point at zero pressure, (2) to monitor those coordinates with increasing pressure, and (3) determine if the transition becomes second-order at high pressure, thus indicating the existence of a tricritical point in the phase diagram of KDP.

A review of recent high precision experiments indicated that even a "simple" dielectric experiment which could meet the above goals

would require temperature resolution on the order of ±2 mK, pressure stability of ±10 ppm at pressures of several kbar, and high impedance static polarization measurements. In addition, measurements would have to be made as near to equilibrium as possible owing to the distortion of results when variables are allowed to drift "quickly" near the transition; this result has long been known to workers in crticial phenomena but has not generally been appreciated by workers in ferroelectricity.

Apparatus was assembled to meet the above requirements. The major components were a two stage cryostat for temperature control, guarded circuitry for polarization charge measurements, a beryllium-copper pressure vessel, and a pressure generating system for application of hydrostatic pressure using He gas.

The temperature and electric field dependence of the net polarization of a KH_2PO_4 crystal was mapped out in the E>0 half plane in a 0.5 K neighborhood of its ferroelectric transition at pressures of 0.0016, 1, and 3 kbar. The data were analyzed by the apparently new technique of considering the T and E dependence along lines of constant polarization, isopols.

2. Conclusions

On the basis of the static measurements of the net polarization of KDP as a function of temperature and electric field in a 0.5 K

neighborhood of its ferroelectric transition at pressures of 0.0016, 1.00, and 3.00 kbar, the following conclusions appear valid.

1. In the paraelectric region the polarization is well described by the Landau equation of state

$$E=A_o(T-T_o)P+BP^3+CP^5$$

to within 0.05 K of the transition temperature at hydrostatic pressures of 0.0016, 1.00, and 3.00 kbar.

2. Based on the best fit Landau parameters to the polarization data on two crystals, the ferroelectric transition is first-order at ambient pressure with the critical point at the termination of the first order line located at $T_{cr}-T_o=0.08\pm0.03$ K and $E_{cr}=200\pm60$ V/cm. This conclusion is supported by increases in the isothermal dielectric constant and the polarization relaxation time constant in the vicinity of the critical point.

3. At 1.00 kbar T_o of sample No. 2 changed by -4.54 ± 0.05 K, and the critical point moved substantially closer to the temperature axis: $T_{cr}-T_o = 0.027 \pm 0.01$ K, $E_{cr}=43\pm13$ V/cm.

4. At 3.00 kbar the transition is second-order as based upon the analysis of isopols which indicates a positive B in the Landau expansion, and supported by the isothermal dielectric constant maximum occurring at E=0.

5. A tricritical point is expected to exist at 2.0±0.5 kbar based upon the interpolated behavior of the best fit Landau parameters as a function of pressure.

3. Significance and Recommendations for Further Study

The results presented in this thesis have significance beyond merely mapping out the phase space of KDP. It is believed that this is the first material with an indicated tricritical point (TCP) whose entire three-dimensional phase space is experimentally accessible. This should allow critical exponents for wing critical points to soon be measured for the first time.

Other members of the KDP family whose transitions are barely first order at ambient pressure (e.g. Cesium Dihydrogen Arsenate) may have TCP's thus allowing the effect, if any, of chemical substitution to be studied. The present result combined with Peercy's[15] recent discovery of a TCP in SbSI, may encourage a search for other ferroelectrics with TCP's. Results from a number of such ferroelectrics would allow further tests of universality.

The fact that the isopol analysis outlined in Chapter III has produced results in good agreement with other methods is significant. Dielectric measurements are in general experimentally simpler at high pressure than neutron or x-ray diffraction, or light scattering techniques. Thus a convenient means is afforded to check

the order of phase transitions which are border-line first or second-order.

As for KDP itself the findings reported here indicate that the transition region around 2 kbar should be thoroughly explored. Taylor expansions of microscopic descriptions of KDP produce a "B" coefficient which is the sum of a number of competing plus and minus terms.[64] Careful measurement of the pressure dependence of microscopic parameters near the transition temperature would aid in the development of a microscopic picture of the TCP.

It is felt that measurements of the noise voltage and current of KDP near the transition might provide an excellent means of identifying both CP's and TCP's. In addition, auto-correlation of the noise voltage should provide a means for direct examination of the correlation time in various regions of the phase space.

It is clear that the final chapter of this investigation has not yet been written.

APPENDIX

Pressure System Manual

This Appendix is not intended as a complete service manual for the entire pressure system. Detailed descriptions of each component, its operation, and repair are given in separate manuals published by the manufacturer. It is suggested that these be consulted before operating any component for the first time.

What this Appendix does contain is an overview of the entire system operation, valve open-closed conditions for various modes of operation, general precautions, and other items peculiar to this system which cannot be found in the manufacturers' literature.

The system consists of two major subsystems: one employing a liquid hydraulic medium at the work point, the other supplying a gas medium. The two subsystems are described separately.

Liquid System

The liquid system is shown in the darker lines of Fig. 17. The hydraulic fluid used to 30 000 psi may be as simple as SAE 10W HD motor oil. Higher pressure, up to 100 000 psi, requires a mixture of 1 part kerosene and 2 parts SAE 10W oil. (Caution: many outlets now sell diesel oil as kerosene. Kerosene is colorless.) Pure 10W oil solidifies at $\gtrsim$50 000 psi causing considerable system damage. Be sure of the pressure medium.

The system should be charged with hydraulic fluid, taking care to remove as much air as possible from the lines. This may be done by cycling the intensifier several times until no air appears at the discharge line or the work point. The procedure is as follows.

Procedure A: Removal of air from liquid system.

1) Close valves V-3, V-4, V-5, and V-7, open V-8 and V-9, and pump with the work point open until no air bubbles appear in the discharge line.

2) Close V-9, open V-5 and continue pumping. This retracts the intensifier. A very rapid permanent pressure increase at gauge G-1 will occur when the intensifier is fully retracted.

3) When the intensifier is fully retracted, close V-5 and V-8, open V-9 and V-4, and pump to advance the intensifier. Again pressure will rise dramatically at the end of the stroke.

4) Repeat the procedure from step 1 until no air appears at the work point or the discharge line at any point of the operation.

Procedure B: Pressure production with the liquid system.

1) Close valves V-3 and V-6.

2) Remove air from system following procedure A.

3) Retract the intensifier: close V-4, V-9, open V-5 and V-8, and pump until a sharp permanent pressure rise occurs at G-1.

4) Close V-4, open V-8 and V-9, and pump to a maximum of 15 000 psi at G-1.

5) If higher pressure is desired, close V-8, and, with V-5 open, open V-4. Now close V-5 and pump to a maximum pressure of 100 000 psi at G-2. N.B. The pressures on G-1 and G-2 should be in the approximate ratio of the intensifier piston areas, 1:23. If this ratio deviates appreciably (say 15%), stop: something is wrong.

6) To relieve the pressure crack V-5 open.

7) If necessary retract the intensifier as per step 3.

Gas System

The gas system is comprised of the lighter lines in Fig. 17. Liquid lines through valve V-3, V-6, and V-7 are also used. Before pressurizing the gas line, one should check that the liquid pressure system has been bled (see procedure A of this Appendix) and that the remote head has been primed (see the manufacturer's manual). The following procedure may then be used to obtain gas pressures to 100 000 psi.

Procedure C: Gas pressurization.

1) Fill the liquid nitrogen trap with liquid nitrogen.

2) Close V-2, V-4, V-5, V-6, V-7, V-8, V-9, VH-2, VP-2, and open VP-1, VH-1, V-1 and V-3.

3) Close the small unlabeled through-valve immediately downstream of the regulator on the He bottle, open the main bottle valve, and set the regulator to 1450 psi.

4) Crack the small through-valve on the regulator open, thereby admitting He to the system. The liquid nitrogen in the trap will boil. When the boiling stops, open the small valve several turns.

5) The system is now pressurized to approximately 1450 psi. At this point the gas intensifier can be retracted if it is not already in its retracted position. A meter showing the position of the intensifier piston in its stroke is located on the front of the pressure panel. Retraction is accomplished by cracking V-7, then waiting for the piston motion to stop. Valves V-7 and V-5 are then opened fully and V-4 cracked, and the intensifier allowed to retract fully. The intensifier is fully retracted when G-1 reads zero and no oil flows in the return line. The object here is to prevent the intensifier from moving too rapidly. The speed is about right when a slow but continuous stream of oil flows in the return line to the reservoir. Valves V-4, V-5 and V-7 should then be closed.

6) The system downstream of the remote head may now be pressurized to 14 000 psi by pumping. Be sure V-6 and V-7 are closed, and V-3 open.

7) If higher pressure is desired, advance the gas intensifier by closing V-3, opening V-7 and pumping.

8) If pressure higher than that attained by a single stroke of the intensifier is desired, the intensifier must be recycled. Carefully note the pressure on G-1.

9) Close VP-1 and retract the intensifier as in step 5.

10) Repressurize the intensifier volume with the remote head as in step 6.

11) Close V-3, open and close V-6, open V-7, and pump to advance the intensifier until the pressure reading on G-1 matches the value noted in step 8. Open VP-1 and continue pumping to increase the pressure at the work point.

12) Repeat steps 8-11 as needed to reach the desired pressure.

The equipment upstream of VH-1 should not be left pressurized for great lengths of time. High pressure gas leaks back through the check valves and the low pressure end of the system can reach pressures great enough to blow the protective rupture disks. The manufacturer also warns against leaving the remote head under pressure. The procedure for venting the low pressure line follows.

Procedure D: Venting the low pressure line.

1) Close the main valve on the supply tank.

2) Crack VH-2, venting the system up to check valve 1.

3) Close VH-1 and complete venting by opening V-2 until the gas bottle regulator reads less than 50 psi.

4) Pressure on the high pressure side of VH-1 may be maintained by periodic pumping on the intensifier through V-7. It has been found that hanging 5 to 20 kg on the end of the pump handle is an aid to

making small pressure corrections when some delicacy but considerable force is needed.

High Pressure Electrical Feedthroughs

Electrical feedthroughs were fabricated from Harwood 3-M stainless steel high-pressure tubing. The tubing was coned and threaded on one end, cut square on the other, and etched inside by heating for 20-30 minutes in a Kel-F beaker containing 25 ml tap water, 10 ml concentrated HNO_3, and 15 ml concentrated HF. The acid solution was periodically circulated through the tubing with an eye dropper. The center conductor was 27 gauge enameled magnet wire. Eccobond 104 epoxy to which 5 percent by weight alumina powder had been added was thoroughly mixed and then out-gassed by pumping on the mixture with a mechanical fore-pump for 15 to 20 min. A Tygon tube was then filled with heated epoxy and attached to the pressure tube by a hose clamp. The epoxy was then squeezed into the stainless-steel tube containing the center wire. After the epoxy set, standard male-to-cable BNC fittings were soldered to the pressure tubing with copper spacers employed to match the pressure tubing OD to the BNC ID. Later experience showed it to be considerably easier to solder the spacers to the tubing before filling the tubing with epoxy. Connection to other male-ended cables was made using a female-female adapter which was never removed from the feedthrough side in order to prevent

straining the somewhat delicate center pin connections on the feedthrough BNC's.

REFERENCES

REFERENCES

[1]H. Eugene Stanley, Introduction to Phase Transitions and Critical Phenomena (Oxford University Press, New York, 1971), Parts I and II.

[2]H. B. Callen, Thermodynamics (Wiley, New York, 1960), Part I.

[3]C. Kittel, Thermal Physics (Wiley, New York, 1969), Chap. 23.

[4]H. A. Leupold, Am. J. Phys. 37, 1047 (1969), Erratum: Am. J. Phys. 39, 1094 (1971).

[5]H. A. Leupold, Am. J. Phys. 39, 1099 (1971).

[6]R. B. Griffiths, Phys. Rev. Letters 24, 715 (1970).

[7]R. B. Griffiths, Phys. Rev. B 7, 545 (1973).

[8]F. J. Wegner and E. K. Riedel, Phys. Rev. B 7, 248 (1973).

[9]L. S. Schulman, Phys. Rev. B 7, 1960 (1973).

[10]E. K. Riedel and F. J. Wegner, Phys. Rev. Letters 29, 349 (1972).

[11]G. Ahlers in The Physics of Liquid and Solid Helium, K. H. Benneman and J. B. Ketterson, Eds. (Wiley, New York, 1976), Vol. I.

[12]N. Giordano and W. P. Wolf, Phys. Rev. Letters 35, 799 (1975).

[13]R. J. Birgeneau, G. Shirane, M. Blume, and W. C. Koehler, Phys. Rev. Letters 33, 1098 (1974).

[14]B. B. Weiner and C. W. Garland, J. Chem. Phys. 56, 155 (1972).

[15]P. S. Peercy, Phys. Rev. Letters 35, 1581 (1975).

[16]V. H. Schmidt, Bull. Am. Phys. Soc. 19, 649 (1974).

[17]G. Busch and P. Scherrer, Naturwiss. 23, 737 (1935).

[18]F. Jona and G. Shirane, Ferroelectric Crystals (Pergamon, Oxford, 1962), Chap. III.

[19]V. H. Schmidt, "Ferroelectric Hydrogen Bonded Systems", in The Hydrogen Bond: Recent Developments in Theory and Experiments, P. Schuster, G. Zundel, and C. Sandorfy, Eds. (North-Holland, Amsterdam, 1976) Vol. III, Chap. 23.

[20]S. W. Peterson, A. H. Levy, and S. H. Simonsen, J. Chem. Phys. 21, 2084 (1953).

[21]Y. Takagi, J. Phys. Soc. Japan 3, 273 (1948).

[22]J. West, Z. Krist 74, 306 (1930).

[23]R. Blinc and S. Svetina, Phys. Rev. 147, 423, 430 (1966).

[24]J. C. Slater, J. Chem. Phys. 9, 16 (1941).

[25]H. B. Silsbee, E. A. Uehling, and V. H. Schmidt, Phys. Rev. 133, A165 (1964).

[26]Collected Papers of L. D. Landau, D. ter Haar, Ed. (Gordon and Breach, New York, 1965), pp. 193-216.

[27]V. L. Ginzburg, Sov. Phys.--Solid State 2, 1824 (1960).

[28]A. F. Devonshire, Advances in Phys. 3, 85 (1954).

[29]J. Grindlay, An Introduction to the Phenomenological Theory of Ferroelectricity (Pergamon Press, Oxford, 1970).

[30]E. Fatuzzo and W. J. Merz, Ferroelectricity, Selected Topics in Solid State Physics, E. P. Wohlfarth, Ed. (Wiley, New York, 1967), Vol. VII, Chap. 3.

[31]L. D. Landau and E. W. Lifshitz, Statistical Physics (Pergamon, London, 1958), Chap. XIV, Section 136.

[32]E. Hegenbarth and S. Ullwer, Cryogenics 7, 306 (1967).

[33]V. G. Vaks and V. I. Zinenko, Sov. Phys.--JETP 37, 330 (1973).

[34]B. A. Strukov, M. A. Korzhuev, A. Baddur, and V. A. Koptsik, Sov. Phys.--Solid State 13, 1569 (1972).

[35]E. V. Sidnenko and V. V. Gladkii, Sov. Phys.--Crystallogr. 18, 83 (1973).

[36]S. R. Garber and L. A. Smolenko, Sov. Phys.--JETP 28, 1072 (1969).

[37]M. Vallade, Phys. Rev. B 12, 3755 (1975).

[38]H. Sugie´, K. Okada and K. Kan'no, J. Phys. Soc. Japan 33, 1727 (1972).

[39]K. Okada, H. Sugie´ and K. Kan'no, Phys. Letters 44A, 59 (1973).

[40]K. Okada and H. Sugie´, International Conference on Soft Modes and Low Lying Vibrational States and Their Relation to Ferroelectricity and Superconductivity (San Juan, Puerto Rico, Dec. 1975), (to be published in Ferroelectrics).

[41]W. Reese, Phys. Rev. 181, 905 (1969).

[42]J. W. Benepe and W. Reese, Phys. Rev. B 3, 3032 (1971).

[43]J. Kobayashi, Y. Utesu, and Y. Enomoto, Phys. Stat. Sol. (b) 45, 293 (1971).

[44]T. Matsuda and R. Abe, J. Phys. Soc. Japan 36, 765 (1973).

[45]J. Eberhard and P. Horn, Solid State Comm. 16, 1343 (1975).

[46]A. B. Western and V. H. Schmidt, Solid State Commun. (to be published).

[47]P. Horn, Private communication.

[48]A. B. Western, A. G. Baker, R. J. Pollina, and V. H. Schmidt, International Conference on Soft Modes and Low Lying Vibrational States and Their Relation to Ferroelectricity and Superconductivity (Dec. 1975), (to be published in Ferroelectrics).

[49]G. Samara, Phys. Rev. Letters 27, 103 (1971).

[50]Interactive Radiation, Inc., 406 Pauling Avenue, Northvale, NJ 07647.

[51]Cleveland Crystals, Inc., Box 3157, Cleveland, Ohio 44117.

[52]Lake Shore Cryotronics, Inc., 9631 Sandrock Road, Eden, NY 14057.

[53]Flexible Silver Coating #16, Hanovia Liquid Gold Division, Engelhard Industries, Inc., East Newark, NJ.

[54]Robert S. Parker, Ph.D. Thesis, Montana State University (unpublished).

[55]W. N. Lawless, Rev. Sci. Instr. 42, 561 (1971).

[56]W. N. Lawless, Rev. Sci. Instr. 46, 625 (1975).

[57]C. B. Sawyer and C. H. Tower, Phys. Rev. 35, 269 (1930).

[58]F. A. Laws, Electrical Measurements (McGraw-Hill, New York, 1917), Chap. IV, pp. 175-7.

[59]E-2512-H, Harwood Engineering Co., Inc., South Street, Walpole, Mass 02081.

[60]Model 250, Precision Temperature Controller, Bayley Instrument Co., Box 605, Danville, CA 94526.

[61]P. Bornarel, A. Fouskova´, P. Guyon, and J. Lajzerowicz, Proceedings of the International meeting on Ferroelectricity (Inst. of Phys. of Czechoslovak Acad. of Sci, Prague, 1966), Vol. II, p. 81.

[62]R. E. Lund, MREG, MATH-STAT library program, Montana State University Computing Center, Bozeman, Montana.

[63]K. Okada and H. Sugie´, Phys. Letters 37A, 337 (1971).

[64]S. Torstveit, private communication.